RENEWABLE ENERGY SYSTEM DESIGN AND OPERATIONAL PLANNING FOR DEMAND FULFILLMENT

A THESIS SUBMITTED TO

THE GRADUATE SCHOOL OF ENGINEERING AND SCIENCE

OF BILKENT UNIVERSITY

IN PARTIAL FULFILLMENT OF THE REQUIREMENTS FOR

THE DEGREE OF

MASTER OF SCIENCE

IN

INDUSTRIAL ENGINEERING

By

Gülin Yurter

August 2024

RENEWABLE ENERGY SYSTEM DESIGN AND OPERATIONAL PLANNING FOR DEMAND FULFILLMENT

By Gülin Yurter

August 2024

We certify that we have read this thesis and that in our opinion it is fully adequate, in scope and in quality, as a thesis for the degree of Master of Science.

Ayşe Selin Kocaman(Advisor)

Emre Nadar(Co-Advisor)

Özlem Karsu

Oktay Karabağ

Approved for the Graduate School of Engineering and Science:

Orhan Arıkan
Director of the Graduate School

ABSTRACT

RENEWABLE ENERGY SYSTEM DESIGN AND OPERATIONAL PLANNING FOR DEMAND FULFILLMENT

Gülin Yurter
M.S. in Industrial Engineering
Advisor: Ayşe Selin Kocaman
Co-Advisor: Emre Nadar
August 2024

Renewable energy sources have gained prominence in reducing the dependency on fossil fuels and minimizing their negative environmental impacts. Considering renewables' uncertain and variable nature, an effective design and operational planning of hybrid energy systems is key to success in clean energy transition. We study the optimal design and operational planning problem of hybrid energy systems involving a renewable energy source and a storage unit. We first develop two-stage stochastic mixed-integer programming models to determine the optimal sizing and investment decisions for solar/wind farms co-operated with pumped hydro energy storage facilities in decentralized areas. We then utilize a Markov decision process to find the optimal energy generation and storage decisions for decentralized grid-connected wind farm-battery systems with demand-fulfillment obligations. This is a novel study that compares several pumped hydro energy storage configurations with respect to optimal sizing decisions for system components and allows for uncertainties in electricity price, wind speed, and electricity demand for optimal operational planning. Using real-life data and considering economic benefits, we demonstrate how the renewable energy systems should be designed and managed to mitigate the adverse effects of uncertainties in matching supply with demand.

Keywords: Renewable energy, hybrid energy systems, energy storage, demand fulfillment, stochastic programming, Markov decision processes.

ÖZET

TALEP KARŞILAMA İÇİN YENİLENEBİLİR ENERJİ SİSTEMLERİ TASARIMI VE YÖNETİMİ

Gülin Yurter
Endüstri Mühendisliği, Yüksek Lisans
Tez Danışmanı: Ayşe Selin Kocaman
İkinci Tez Danışmanı: Emre Nadar
Ağustos 2024

Fosil yakıtlara olan bağlılığın ve onların çevreye olan olumsuz etkilerinin azaltılması adına yenilenebilir enerji kaynakları önem kazanmaktadır. Bu kaynakların belirsiz ve değişken doğası göz önüne alındığında, hibrit enerji sistemlerinin tasarlanması ve yönetilmesi, temiz enerji dönüşümünde başarının anahtarıdır. Bu çalışmada, hibrit enerji sistemlerinin en uygun tasarımı ve yönetimi konusu bir enerji depolama sistemi ile birlikte çalışan bir yenilenebilir enerji kaynağı üzerinden incelenmektedir. Öncelikle, iki aşamalı stokastik karışık tamsayılı programlama modelleri kullanılarak merkezi olmayan bölgede pompaj depolamalı sistemle birlikte çalışan güneş/rüzgar çiftliği için en uygun boyutlandırma ve yatırım kararları ele alınmaktadır. Sonrasında, bir Markov karar süreci kullanılarak rüzgar çiftliği ve bataryadan oluşan merkezi olmayan bir bölge için talebin karşılanması ve en iyi üretim ve depolama kararlarının bulunması amaçlanmaktır. Bu özgün çalışma, çeşitli pompaj depolamalı sistemleri bileşen boyutları açısından karşılaştırmakta ve elektrik fiyatı, rüzgar hızı ve elektrik talebindeki belirsizlikleri operasyonel planlamaya dahil etmektedir. Gerçek veriler kullanılarak ve ekonomik katkılara odaklanılarak, yenilenebilir enerji sistemlerinin arz ve talep eşleştirmesindeki belirsizliklerin olumsuz etkilerini nasıl azaltabileceği gösterilmektedir.

Anahtar sözcükler: Yenilenebilir enerji, hibrit enerji sistemleri, enerji depolama, talep karşılama, stokastik programlama, Markov karar süreçleri.

Acknowledgement

I would like to begin by expressing my sincere gratitude to my advisors, Assoc. Prof. Ayşe Selin Kocaman and Asst. Prof. Emre Nadar. Their endless support, guidance, and the opportunities they provided over the past two years have been instrumental in my academic development and personal growth. It has been a great pleasure and privilege to work under the supervision of such kind-hearted mentors.

I also want to thank Asst. Prof. Oktay Karabağ and Assoc. Prof. Özlem Karsu for accepting to read and review my thesis, providing valuable feedback, and offering insightful comments. I would also like to thank all the professors and staff in the Department of Industrial Engineering for their help and support.

I am indebted to Ece Çiğdem Karakoyun and Parinaz Toufani for their willingness to help whenever needed. My appreciation also extends to Zehranaz Varol and Deniz Akkaya for their guidance and support as fellow PhD students in our department.

I am extremely grateful to my friends Elif Rana Yöner, Deniz Şahin, Göksu Ece Okur, Doğuş Berk Koçak, Gözde Yazıcı, and Ali İlhan Haliloğlu. They made this challenging journey enjoyable. I also deeply appreciate the support of my dear friends İpek Şahin, Ecem Yücel, and Öykü Hatipoğlu. I also want to thank Onur Erdoğan for believing in me, especially during times when I struggled to believe in myself.

Finally, I want to express my deepest gratitude to my beloved parents, Hayat Yurter and Uğur Yurter. Their unconditional love, understanding, and support have been the foundation of everything I have achieved. This thesis is dedicated to them, and to my grandparents, Güner Erdem and Hidayet Erdem, whose genuine interest in my work and eagerness to listen to my progress have meant so much to me. Their support and encouragement have been a source of inspiration and motivation throughout my academic journey.

Contents

List of Figures

List of Tables

Chapter 1

Introduction

The use of fossil fuels increases greenhouse gas emissions and threatens the achievement of Sustainable Development Goal 7 (SDG7) that has been set to "ensure access to affordable, reliable, sustainable, and modern energy for all" [2]. Renewable energy sources like hydropower, wind, and solar provide cleaner alternatives to fossil fuels in addressing the problems mentioned above. However, the transition from fossil fuels to renewable energy sources presents a significant challenge due to the intermittent and variable nature of renewables. For example, the solar energy production depends on solar irradiation that varies during the day and is affected by weather conditions like cloud cover or air quality. Similarly, the wind energy production hinges upon wind availability and wind speed that can change rapidly and are difficult to predict. When there is less sunlight or wind, the renewable energy output can drop significantly, leading to energy supply shortages and obstructing consistent and reliable energy supply (i.e., the grid instability). The periods of overproduction as well as underproduction may arise from the variable output of renewable energy sources, placing a burden on energy management systems and causing inefficiencies. Consequently, the renewable energy systems can sometimes be unreliable and in certain situations unsustainable, making it difficult to achieve the SDG7.

The system flexibility is mandatory to ensure reliability and sustainability.

The energy storage systems are introduced to provide this flexibility [3]. In such systems, the energy balance is consistently maintained, and the system quality and efficiency are fortified when there is energy storage [4]. According to Peng et al. [5], storage and renewables can be substitutes when meeting peak demand, and understanding these effects would allow the decision-makers to optimize their investment and operational planning decisions for energy systems. Kaushik et al. [6] provide an overview of recent developments in commercial renewables, hybrid energy resources, storage units, and energy management strategies. Considering the necessity of transition from fossil fuels to renewables and the need for storage to mitigate the anticipated challenges, this thesis combines two studies: one on the design problem and one on the operational planning problem for renewable energy systems with storage units.

The first study considers a pumped hydro energy storage (PHES) system that can be installed in various configurations depending on the specific geographical and hydrological conditions. Closed-loop PHES systems are off-stream and have no natural inflow to the system. However, open-loop systems are on-stream and have natural inflows to the upper and/or lower reservoirs. In this study, we develop two-stage stochastic programming models for various PHES configurations to investigate how the choice of PHES configuration impacts the sizing decisions and costs of a hybrid system that includes a renewable power generator co-operated with PHES. Our numerical results show that using a PHES facility instead of a conventional hydropower system reduces the expected system cost and mismatched demand significantly. Open-loop PHES facilities perform better than closed-loop PHES and seawater-PHES facilities, dramatically lowering the need for fossil fuels in demand fulfillment. The most cost-efficient PHES configuration is when there is natural inflow to the upper reservoir. Using solar energy instead of wind as the renewable source significantly increases the requirement for larger upper reservoirs in on-stream open-loop PHES facilities, while reducing the expected system cost for all configurations.

The second study considers the operational planning problem for a wind farm co-operated with a battery in a decentralized grid-connected region. In this setting, the system operator has the primary obligation to fulfill the decentralized-area demand. The energy required to meet the demand can be generated from the wind farm and/or the battery. The system operator can purchase energy from the market if the available energy is insufficient to meet the demand. The system operator can also sell and purchase energy for energy arbitrage purposes. We model the uncertainties in electricity price, electricity demand, and wind speed, formulate the problem as a Markov decision process (MDP), and solve it using a backward dynamic programming algorithm. Our results show that the substitution effect among different system components provide flexibility in the system design choice: Different system configurations may yield similar revenues with different operational implications. The impact of demand-fulfillment obligation on revenues is more significant for small systems. The absence of wind energy generation may render the energy arbitrage gains insufficient for positive cash flows. We also examine the value of including uncertainties in our setting and observe that uncertainty modeling plays a more critical role under renewable energy scarcity.

This thesis makes two significant contributions to the literature. First, we present a comprehensive comparison of various PHES configurations by focusing on the streamflow uncertainty via two-stage stochastic mixed-integer programming models and determining the optimal component sizes of different system configurations. Second, we address the energy generation and storage problem for renewable energy system operators by considering the decentralized grid-connected wind farm-battery setting with demand-fulfillment obligation and employing the MDP methodology to effectively incorporate the price, demand, and wind uncertainties.

The outline of this thesis is as follows: Chapter 2 considers the PHES design problem with two-stage stochastic mixed-integer programming formulations. Chapter 3 considers the wind farm-battery operational planning problem with an MDP formulation. Chapter 4 provides a concluding summary.

Chapter 2

The Impact of Pumped Hydro Energy Storage Configurations on Investment Planning of Hybrid Systems with Renewables

2.1 Introduction

In recent years, renewable energy sources have received significant attention so as to reduce reliance on fossil fuels and mitigate their negative environmental impacts. Nearly two-thirds of the global power capacity additions are for wind and solar [7]. However, given the intermittent nature of these sources, it is necessary to support them with efficient and flexible storage systems to enhance their reliability. One such solution is pumped hydro energy storage (PHES), which stands out as one of the most widely adopted large-scale storage technologies to address the intermittency challenge of renewable sources [8]. PHES systems pump water to an elevated reservoir to store any available excess energy. This stored energy can be retrieved by releasing water from the upper reservoir to a lower one. Thanks to its superior environmental and financial performance when compared to many other storage technologies, PHES has emerged as one of the most commercially viable storage options [9] and accounts for 96% of the global power storage capacity [7].

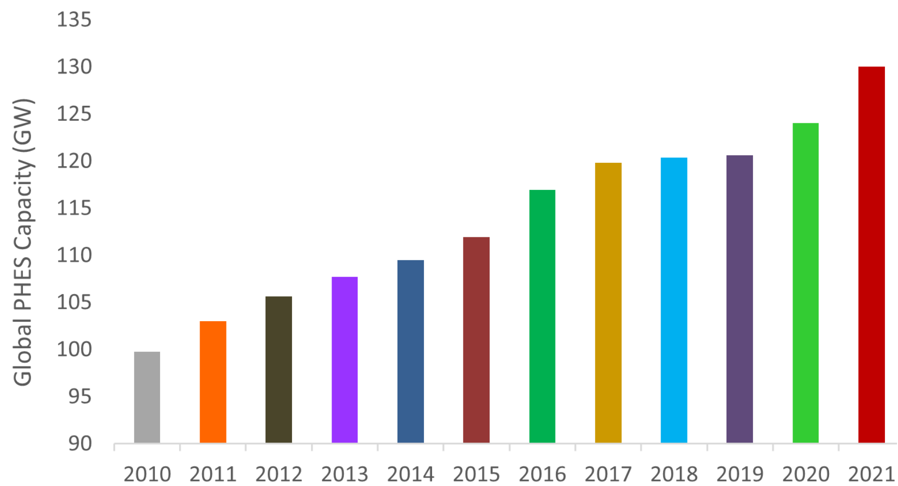

Figure 2.1: Installed PHES capacity from 2010 to 2021 (GW) [1].

The global installed capacity of PHES systems has shown a rapid increase in the past decade and has reached 130 GW in 2021 [10]. Figure 2.1 exhibits this trend from 2010 to 2021. The distribution of the rated PHES capacity across different regions of the world can be observed in Figure 2.2. The rapid expansion of PHES capacity in recent years has been accompanied by a significant increase in regional disparities. According to the International Renewable Energy Agency (IRENA), Asia currently has the highest PHES capacity in the world with a rated power of 72 GW, followed by Europe and North America with capacities of 28 GW and 22 GW, respectively. Africa and the Middle East lag far behind with capacities of 3.2 GW and 1.5 GW, respectively [1]. IRENA also reports that China leads the world with a capacity of 36 GW, followed by Japan with a capacity of 22 GW [1]. In North America, the United States has a capacity of 22 GW, while Canada lags behind with a capacity of only 177 MW [1, 11]. Although Canada is the world's fourth-largest hydropower generator with a capacity of 81 GW as of 2019, its PHES capacity is limited [10].

While conventional hydropower remains of great interest globally with a capacity of 1360 GW in 2021 [10], the PHES systems have been gaining importance

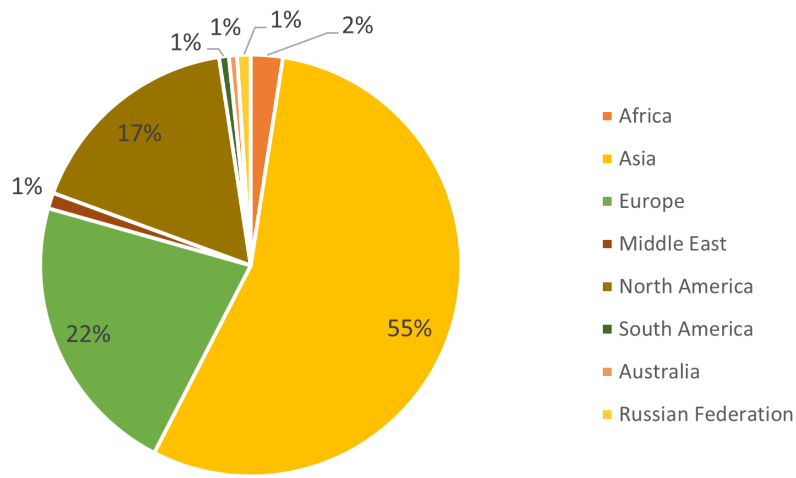

Figure 2.2: Global PHES capacity distribution [1].

due to their potential to reduce the use of nonrenewable resources and improve load-balancing and resource allocation [12]. The growth trend of PHES systems is expected to continue as this technology becomes more widely recognized as a valuable tool for energy storage and grid stabilization. The PHES systems are typically classified into two primary types based on geographical conditions and natural water availability: open-loop vs. closed-loop [13]. Open-loop PHES systems rely on natural water inflow to supply upper and/or lower reservoirs, while closed-loop PHES operations are independent of the natural water inflow. In this chapter, we develop two-stage stochastic programming models for various PHES configurations to investigate how the choice of PHES configuration impacts the sizing decisions and costs of a hybrid system that includes a renewable source co-operated with PHES.

Considering the intermittencies of renewable resources and the uncertainties associated with them, it is a non-trivial task to optimize the sizing and operational decisions of hybrid energy systems with PHES. We refer the reader to Mahfoud et al. [14] and Toufani et al. [15] for comprehensive reviews of the PHES literature. In this literature, there are relatively fewer studies that model PHES systems via stochastic optimization frameworks, compared to deterministic approaches. The majority of stochastic optimization models focus only on the operational decisions of existing PHES systems. Two important examples of this category, which also motivated this chapter, are proposed by Toufani et al. [16, 17]. Toufani et al. [16] examine the energy generation and storage problem for alternative PHES facilities (i.e., open-loop facilities with natural water inflow to upper and/or lower reservoirs and closed-loop facilities), formulating the problem as a stochastic dynamic program. Toufani et al. [17] study the energy generation and storage problem to evaluate the benefits of transforming conventional cascade hydropower stations into PHES systems, again modeling this operational problem as a stochastic dynamic program.

Optimizing the operations of hybrid energy systems with PHES is crucial for efficient control and management. However, it is equally important to devise an optimal sizing plan under uncertainty to ensure a sufficient power supply without incurring excessive costs during the entire life cycle of the facility. In the literature dealing with the sizing problem under uncertainty, Zheng et al. [18] compare the dispatch strategies of various storage facilities, including a PHES facility. Brown et al. [19] address the question of how much pumped storage capacity to install for a PHES facility in a small island system. Reuter et al. [20] evaluate the economics of PHES systems with wind farms to stabilize profits from wind. Hemmati [21] proposes a renewable energy hub composed of wind-hydro-solar generation systems, supported by PHES and hydrogen storage systems, and optimizes system component capacities and operations to meet demand in autonomous buildings. Liu et al. [22] study the sizing problem for hydro-photovoltaic (PV)-pumped storage integrated generation system by taking into account the uncertainties in PV, spot price, and load. Elnozahy et al. [23] consider different hybrid storage options, including a PHES facility, by incorporating the weather uncertainty into a chance constraint. Abdalla et al. [24] study the sizing problem for wind-PHES systems by taking into account the wind and price uncertainties in their two-stage robust expansion planning model. Amusat et al. [25] solve a bi-criteria sizing problem to demonstrate the effects of intermittency and inter-year variability of renewable sources for several storage options, including a PHES facility. Within a hybrid system incorporating PV panels and a costly diesel backup source, Kocaman and Modi [12] examine the value of a particular PHES configuration compared to a conventional hydropower station. Finally, Kocaman [26] presents two-stage stochastic programming models for mixed (a form of open-loop configuration) and pure (also known as seawater PHES configuration) PHES systems to study the sizing problem for hybrid energy systems.

In this chapter, unlike Kocaman [26], we construct two-stage stochastic mixed-integer programming models for three different configurations of open-loop PHES systems: (i) the natural water flows only into the upper reservoir, (ii) it flows only into the lower reservoir, or (iii) it flows into both reservoirs. Furthermore, again unlike Kocaman [26], we extend these models to closed-loop, seawater and conventional hydropower systems (with no pumping capability). All these configurations are shown in Figure 2.3. We study the sizing problem for these different configurations when they are integrated with a renewable source (solar or wind). The primary contributions of this chapter can be summarized as follows:

- Our study is the first to compare various open-loop PHES configurations (on-stream systems with natural inflow to upper and/or lower reservoirs) in terms of the optimal sizing decisions for system components. We also compare these configurations against closed-loop PHES facilities with capacitated lower reservoir, seawater-PHES facilities, and conventional hydropower systems. We perform all these comparisons in two different cases: when the hybrid energy system includes a solar farm or a wind farm.

- We develop two-stage stochastic mixed-integer programming models to optimize the sizing decisions for system components (e.g., the reservoir and generator capacities, solar panel area, and number of wind turbines) as well as the operational decisions (e.g., the amount of water to be pumped or released and the amount of energy to be curtailed).

- In our numerical experiments, we use real time-series data to take into account the streamflow uncertainty and measure the value of stochastic solution. With our numerical results, we offer new insights into the sizing decisions and costs of hybrid energy systems in different environments.

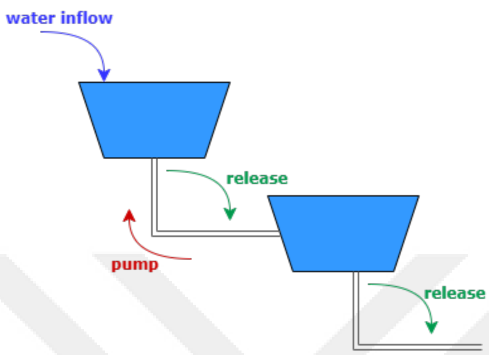

(a) Water inflow to the upper reservoir

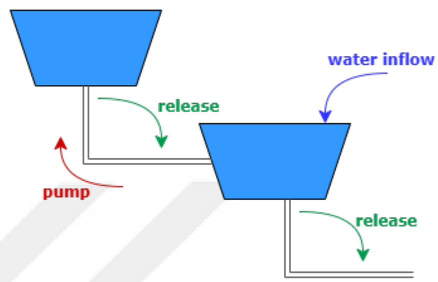

(b) Water inflow to the lower reservoir

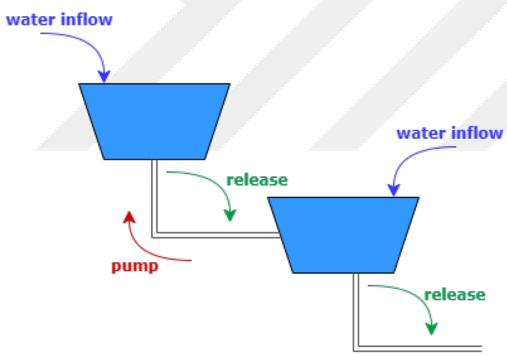

(c) Water inflow to both reservoirs

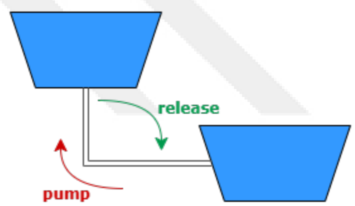

(d) Closed-loop with capacitated lower reservoir

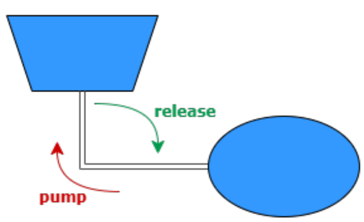

(e) Seawater

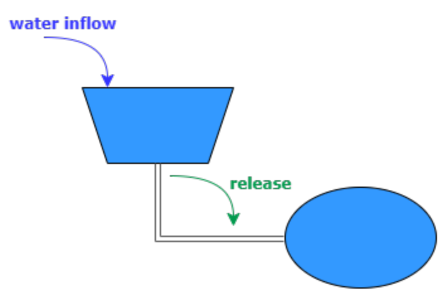

(f) Conventional

Figure 2.3: (a)-(e) possible PHES configurations, (f) conventional hydropower station.

The rest of this chapter is organized as follows: Section 2.2 formulates the two-stage stochastic programs for the sizing and operational planning problems of different PHES configurations. Section 2.3 presents the numerical results and their discussions. Section 2.4 presents the sensitivity results. Section 2.5 concludes by offering a summary.

2.2 Problem Formulation

Our focus is on determining the optimal sizing of the hybrid system components (the PHES facility and the wind/solar farm) and the transmission line between the PHES facility and demand points. Figure 2.4 illustrates a hybrid energy system with a specific PHES configuration. In this system, the natural water flows into both reservoirs of the PHES facility and the hydropower generated can be transmitted to the demand points. Excess renewable energy generated in the demand points can be transmitted to the PHES facility to pump water from the lower reservoir to the upper reservoir to store it as gravitational potential energy. When the available renewable energy is not sufficient to meet the entire demand, we allow for a mismatch between supply and demand and a non-renewable resource like diesel can be used as a substitute. Like [12], we take the cost of diesel as the penalty for any mismatched demand, which is charged for each kWh of energy demand that hydropower or wind/solar power cannot meet.

2.2.1 Assumptions

In order to simplify the modeling of hydropower components, we make several commonly-used assumptions. Specifically, we assume that the water is always released from a constant height, the system efficiency is not affected by the amount of water pumped or released, and there is no loss of water in the PHES facility due to evaporation [27, 26]. We consider a one-year planning horizon to capture the seasonal variability of renewable energy sources. We consider hourly energy generation and storage decisions to capture the intraday supply/demand variability. Since there is significant solar variability throughout the day, the use of hourly periods is needed [12]. Therefore, like [12], we employ a scenario-based model for the problem and utilize a one-year series with hourly periods.

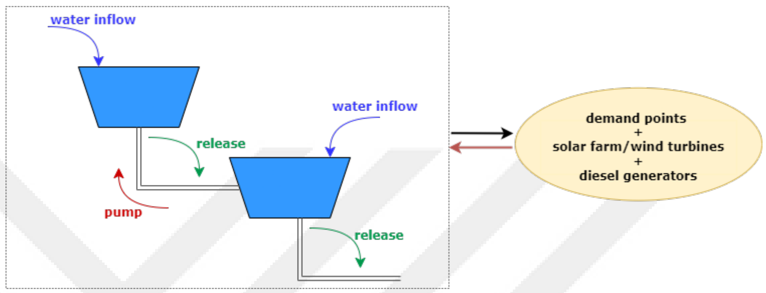

Figure 2.4: A sample hybrid system with an open-loop PHES facility.

2.2.2 Two-stage stochastic programming model

The two-stage stochastic programming model consists of two decision-making stages. The first-stage decisions x are made before the uncertainty is resolved, while the second-stage decisions y are made based on the observed uncertainty. We can formulate the two-stage stochastic program in standard form as follows:

$$\min\ c^T x + \mathbb{E}_\omega[Q(x,\omega)] \tag{2.1}$$

$$\text{s.t. } Ax = b, \tag{2.2}$$

$$x \geq 0. \tag{2.3}$$

In the above formulation $Q(x,\omega)$ is the optimal solution to the second-stage problem with scenario ω. When there is a finite number of scenarios (realizations) and (d,h,T,W) is the data for the second-stage problem, we can find $Q(x,\omega)$ as follows [26, 28]:

$$Q(x,\omega) = \min\{d_\omega^T y_\omega | T_\omega x + W_\omega y_\omega = h_\omega, y_\omega \geq 0\}. \tag{2.4}$$

The extended form of the scenario-based two-stage stochastic program can be written as follows:

$$\min\ c^T x + \sum_{\omega} p_\omega d_\omega^T y_\omega \tag{2.5}$$

$$\text{s.t. } Ax = b, \tag{2.6}$$

$$T_\omega x + W_\omega y_\omega = h_\omega \quad \forall \omega, \tag{2.7}$$

$$x \geq 0,\ y_\omega \geq 0 \quad \forall \omega. \tag{2.8}$$

For our problem, the first-stage decisions involve the sizing decisions for the system components, while the second-stage decisions involve the operational decisions that depend on the observed scenario. To address our research question, we construct two-stage stochastic programming models for each of the six different system configurations, including the conventional hydropower station in addition to five different PHES configurations. Indices, parameters, and decision variables of these models are given in Tables 2.1–2.3.

Table 2.1: Indices for parameters and decision variables.

t	time period 1,...,T, with a total of T periods
ω	scenario 1,...,Ω, with a total of Ω scenarios

Table 2.2: Model parameters.

n	length of each time period
d_h	dimensionless annualization parameter for PHES systems
d_s	dimensionless annualization parameter for solar power stations
d_w	dimensionless annualization parameter for wind power stations
d_t	dimensionless annualization parameter for transmission lines
l	percentage power loss in transmission lines
g	standard acceleration due to gravity
h_U	height of the upper reservoir in the PHES system
h_L	height of the lower reservoir in the PHES system
$dist$	distance between the demand point and the PHES system
α	efficiency of the PHES system in both generation and pump modes
γ	efficiency of solar panels
c_H	unit cost of reservoir capacity in hydropower station
c_{PG}	unit cost of generator/pump capacity in hydropower station
c_S	unit cost of solar panels
c_W	unit cost of wind turbines
c_T	unit cost of transmission line between the PHES system and the demand point
μ	unit penalty for mismatched demand
p_ω	weight of scenario ω, where $\sum_{\omega=1}^{\Omega} p_\omega = 1$
M	a large number

Table 2.3: Model variables.

Exogenous variables	
$SR^{t\omega}$	solar radiation in period t in scenario ω
$WE^{t\omega}$	energy generated from one wind turbine in period t in scenario ω
$ED^{t\omega}$	energy demand in period t in scenario ω
$WU^{t\omega}$	streamflow amount into the upper reservoir in period t in scenario ω
$WL^{t\omega}$	streamflow amount into the lower reservoir in period t in scenario ω
Decision variables	
$S_{U_{max}}$	upper reservoir capacity
$S_{L_{max}}$	lower reservoir capacity
$PG_{U_{max}}$	upper generator capacity
$PG_{L_{max}}$	lower generator capacity
T_{max}	transmission line capacity
A	solar panel area
N	number of wind turbines
$S_U^{t\omega}$	water stored in the upper reservoir at the end of period t in scenario ω
$S_L^{t\omega}$	water stored in the lower reservoir at the end of period t in scenario ω
$P^{t\omega}$	water pumped to the upper reservoir in period t in scenario ω
$R_U^{t\omega}$	water released from the upper reservoir in period t in scenario ω
$R_L^{t\omega}$	water released from the lower reservoir in period t in scenario ω
$V^{t\omega}$	solar energy directly used in the demand points in period t in scenario ω
$IP^{t\omega}$	binary variable which is equal to 1 during pumping and equal to 0 during releasing in period t in scenario ω
$Z^{t\omega}$	mismatched demand in period t in scenario ω
$L_U^{t\omega}$	water spilled from the upper reservoir in period t in scenario ω
$L_L^{t\omega}$	water spilled from the lower reservoir in period t in scenario ω
$C^{t\omega}$	curtailed renewable energy in period t in scenario ω

We present below our stochastic programming model for the hybrid system that includes the most general PHES configuration (i.e., an open-loop PHES system with water inflow to both upper and lower reservoirs) and a solar farm:

$$\text{minimize } d_h c_H(S_{U_{max}} + S_{L_{max}}) + d_h c_{PG}(PG_{U_{max}} + PG_{L_{max}}) + d_s c_S A + dist \cdot d_t c_T T_{max} + \frac{\mu}{\Omega} \sum_{\omega=1}^{\Omega} \sum_{t=1}^{T} Z^{t\omega} \tag{2.9}$$

subject to

$$S_U^{t\omega} = S_U^{t-1,\omega} + WU^{t\omega} + P^{t\omega} - R_U^{t\omega} - L_U^{t\omega} \quad \forall t > 1,\ \forall \omega, \tag{2.10}$$

$$S_L^{t\omega} = S_L^{t-1,\omega} + WL^{t\omega} - P^{t\omega} + R_U^{t\omega} - R_L^{t\omega} + L_U^{t\omega} - L_L^{t\omega} \quad \forall t > 1,\ \forall \omega, \tag{2.11}$$

$$S_U^{1\omega} = \frac{S_{U_{max}}}{2} + WU^{1\omega} + P^{1\omega} - R_U^{1\omega} - L_U^{1\omega} \quad \forall \omega, \tag{2.12}$$

$$S_L^{1\omega} = \frac{S_{L_{max}}}{2} + WL^{1\omega} - P^{1\omega} + R_U^{1\omega} - R_L^{1\omega} + L_U^{1\omega} - L_L^{1\omega} \quad \forall \omega, \tag{2.13}$$

$$S_U^{T\omega} = \frac{S_{U_{max}}}{2} \quad \forall \omega, \tag{2.14}$$

$$S_L^{T\omega} = \frac{S_{L_{max}}}{2} \quad \forall \omega, \tag{2.15}$$

$$S_U^{t\omega} \le S_{U_{max}} \quad \forall t,\ \forall \omega, \tag{2.16}$$

$$S_L^{t\omega} \le S_{L_{max}} \quad \forall t,\ \forall \omega, \tag{2.17}$$

$$\max\left\{R_U^{t\omega} g h_U \alpha, \frac{P^{t\omega} g h_U}{\alpha}\right\} \le PG_{U_{max}} n \quad \forall t,\ \forall \omega, \tag{2.18}$$

$$R_L^{t\omega} g h_L \alpha \le PG_{L_{max}} n \quad \forall t,\ \forall \omega, \tag{2.19}$$

$$\max\left\{(R_U^{t\omega} h_U + R_L^{t\omega} h_L) g \alpha, \frac{P^{t\omega} g h_U}{\alpha(1-l)}\right\} \le T_{max} n \quad \forall t,\ \forall \omega, \tag{2.20}$$

$$V^{t\omega} + \frac{P^{t\omega} g h_U}{\alpha(1-l)} + C^{t\omega} = A\gamma(SR^{t\omega}) \quad \forall t,\ \forall \omega, \tag{2.21}$$

$$ED^{t\omega} = Z^{t\omega} + V^{t\omega} + (R_U^{t\omega} h_U + R_L^{t\omega} h_L) g \alpha (1-l) \quad \forall t,\ \forall \omega, \tag{2.22}$$

$$P^{t\omega} \le IP^{t\omega} M \quad \forall t,\ \forall \omega, \tag{2.23}$$

$$R_U^{t\omega} \le (1 - IP^{t\omega}) M \quad \forall t,\ \forall \omega, \tag{2.24}$$

$$R_L^{t\omega} \leq (1 - IP^{t\omega})M \quad \forall t,\ \forall \omega, \tag{2.25}$$

$$IP^{t\omega} \in \{0, 1\} \quad \forall t,\ \forall \omega, \tag{2.26}$$

$$\begin{aligned} &L_U^{t\omega}, L_L^{t\omega}, S_U^{t\omega}, S_L^{t\omega}, S_{U_{max}}, S_{L_{max}}, PG_{U_{max}}, PG_{L_{max}}, \\ &T_{max}, A, P^{t\omega}, R_U^{t\omega}, R_L^{t\omega}, V^{t\omega}, Z^{t\omega}, C^{t\omega} \geq 0 \quad \forall t,\ \forall \omega. \end{aligned} \tag{2.27}$$

The objective in equation (2.9) is to minimize the total system cost that includes the installation costs and the penalty costs for mismatched demand. For the installation costs, we multiply the sizes of all system components (upper and lower reservoirs, generators, solar panels, and transmission lines) by their unit installation costs and dimensionless annualization parameters. For the penalty costs, we calculate the total mismatched demand in each scenario, take the average over all scenarios, and multiply it by the unit penalty cost.

Equations (2.10) and (2.11) are the flow balance equations for the upper and lower reservoirs. We assume that both reservoirs are half-full at the beginning and end of the planning horizon. We incorporate this assumption into the flow balance equations with equations (2.12) and (2.13) in the first period and with equations (2.14) and (2.15) in the last period. Equations (2.16)-(2.20) set the capacity constraints for the upper and lower reservoirs, generators, transmission lines, respectively. Equation (2.21) ensures that the solar energy potential in any period is equal to the total amount of solar energy that is directly used to meet demand, utilized to pump water in the PHES facility, or curtailed in that period. Equation (2.22) ensures that the demand is met by the hydro or solar energy generated, taking into account any mismatched demand. Together with equation (2.26), equations (2.23), (2.24) and (2.25) are logical constraints that prohibit simultaneous pumping and releasing, affecting only the operational decisions.

2.2.3 Formulations for the alternative systems

2.2.3.1 Water inflow to the upper reservoir

When there is water inflow only to the upper reservoir, we update only the constraints that include the decision variable related to water inflow to the lower reservoir.

minimize (2.9)
subject to

$$S_U^{t\omega} = S_U^{t-1,\omega} + WU^{t\omega} + P^{t\omega} - R_U^{t\omega} - L_U^{t\omega} \quad \forall t > 1, \ \forall \omega,$$

$$S_L^{t\omega} = S_L^{t-1,\omega} - P^{t\omega} + R_U^{t\omega} - R_L^{t\omega} + L_U^{t\omega} - L_L^{t\omega} \quad \forall t > 1, \ \forall \omega,$$

$$S_U^{1\omega} = \frac{S_{U_{max}}}{2} + WU^{1\omega} + P^{1\omega} - R_U^{1\omega} - L_U^{1\omega} \quad \forall \omega,$$

$$S_L^{1\omega} = \frac{S_{L_{max}}}{2} - P^{1\omega} + R_U^{1\omega} - R_L^{1\omega} + L_U^{1\omega} - L_L^{1\omega} \quad \forall \omega,$$

$$(2.14) - (2.27).$$

2.2.3.2 Water inflow to the lower reservoir

minimize (2.9)
subject to

$$S_U^{t\omega} = S_U^{t-1,\omega} + P^{t\omega} - R_U^{t\omega} - L_U^{t\omega} \quad \forall t > 1, \ \forall \omega,$$

$$S_L^{t\omega} = S_L^{t-1,\omega} + WL^{t\omega} - P^{t\omega} + R_U^{t\omega} - R_L^{t\omega} + L_U^{t\omega} - L_L^{t\omega} \quad \forall t > 1, \ \forall \omega,$$

$$S_U^{1\omega} = \frac{S_{max}}{2} + P^{1\omega} - R_U^{1\omega} - L_U^{1\omega} \quad \forall \omega,$$

$$S_L^{1\omega} = \frac{S_{L_{max}}}{2} + WL^{1\omega} - P^{1\omega} + R_U^{1\omega} - R_L^{1\omega} + L_U^{1\omega} - L_L^{1\omega} \quad \forall \omega,$$

$$(2.14) - (2.27).$$

2.2.3.3 Closed-loop PHES facilities

Closed-loop PHES facilities have no natural water inflow. There is no water spillage in either reservoir and there is no power generator in the lower reservoir.

$$\text{minimize } d_h c_H (S_{U_{max}} + S_{L_{max}}) + d_h c_{PG} PG_{U_{max}} + \; d_s c_S A + dist \cdot d_t c_T T_{max} \\ + \frac{\mu}{\Omega} \sum_{\omega=1}^{\Omega} \sum_{t=1}^{T} Z^{t\omega}$$

subject to

$$\begin{aligned}
S_U^{t\omega} &= S_U^{t-1,\omega} + P^{t\omega} - R_U^{t\omega} \quad \forall t > 1, \; \forall \omega, \\
S_L^{t\omega} &= S_L^{t-1,\omega} - P^{t\omega} + R_U^{t\omega} \quad \forall t > 1, \; \forall \omega, \\
S_U^{1\omega} &= \frac{S_{U_{max}}}{2} + P^{1\omega} - R_U^{1\omega} \quad \forall \omega, \\
S_L^{1\omega} &= \frac{S_{L_{max}}}{2} - P^{1\omega} + R_U^{1\omega} \quad \forall \omega, \\
\max \left\{ R_U^{t\omega} hg\alpha, \frac{P^{t\omega} gh}{\alpha(1-l)} \right\} &\leq T_{max} n \quad \forall t, \; \forall \omega, \\
ED^{t\omega} &= Z^{t\omega} + V^{t\omega} + R_U^{t\omega} hg\alpha(1-l) \quad \forall t, \; \forall \omega, \\
&(2.14) - (2.18), \; (2.21), \; (2.23) - (2.27).
\end{aligned}$$

2.2.3.4 Seawater-PHES facilities

The seawater-PHES facilities are similar to the closed-loop PHES facilities, with the exception that the lower reservoir has no specified capacity and is regarded as a sea. We thus no longer include the decision variables $S_L^{t\omega}$ and $S_{L_{max}}$ in our model. We note that this configuration is equivalent to the pure PHES configuration in

[26].

$$\text{minimize } d_h c_H S_{\max} + d_h c_{PG} PG_{U_{\max}} + d_s c_S A + dist \cdot d_t c_T T_{\max} + \frac{\mu}{\Omega} \sum_{\omega=1}^{\Omega} \sum_{t=1}^{T} Z^{t\omega}$$

subject to

$$S^{t\omega} = S^{t-1,\omega} + P^{t\omega} - R_U^{t\omega} \quad \forall t > 1,\ \forall \omega,$$
$$S^{1\omega} = \frac{S_{max}}{2} + P^{1\omega} - R_U^{1\omega} \quad \forall \omega,$$
$$\max\left\{ R_U^{t\omega} hg\alpha, \frac{P^{t\omega} gh}{\alpha(1-l)} \right\} \le T_{max} n \quad \forall t,\ \forall \omega,$$
$$ED^{t\omega} = Z^{t\omega} + V^{t\omega} + R_U^{t\omega} hg\alpha(1-l) \quad \forall t,\ \forall \omega,$$
$$(2.14),\ (2.16),\ (2.18),\ (2.21),\ (2.23) - (2.27).$$

2.2.3.5 Conventional hydropower stations

The conventional hydropower stations have no pumping capability and no lower reservoir. We thus remove the decision variables $S_{L_{max}}$, PG_L^{max}, $S_L^{t\omega}$, $P^{t\omega}$, $R_L^{t\omega}$, and $L_L^{t\omega}$ from our model.

$$\text{minimize } d_h c_H S_{max} + d_h c_{PG} PG_{max} + \ d_s c_S A + dist \cdot d_t c_T T_{max} + \frac{\mu}{\Omega} \sum_{\omega=1}^{\Omega} \sum_{t=1}^{T} Z^{t\omega}$$

subject to

$$S^{t\omega} = S^{t-1\omega} + WU^{t\omega} - R_U^{t\omega} - L_U^{t\omega} \quad \forall t > 1,\ \forall \omega,$$
$$S^{1\omega} = \frac{S_{max}}{2} + WU^{1\omega} - R_U^{1\omega} - L_U^{1\omega} \quad \forall \omega,$$
$$R_U^{t\omega} gh\alpha \le PG_{max} n \quad \forall t,\ \forall \omega,$$
$$R_U^{t\omega} gh\alpha \le T_{max} n \quad \forall t,\ \forall \omega,$$
$$ED^{t\omega} = Z^{t\omega} + V^{t\omega} + R_U^{t\omega} gh\alpha(1-l) \quad \forall t,\ \forall \omega,$$

$$(2.14),\ (2.16),\ (2.21),\ (2.27).$$

2.2.4 Hybrid systems with wind farms

If the hybrid energy system includes a wind farm instead of a solar farm, equation (2.21) of our main model can be modified as follows:

$$V^{t\omega} + \frac{P^{t\omega}gh}{\alpha(1-l)} + C^{t\omega} = WE^{t\omega}N \quad \forall t,\ \forall\omega, \tag{2.28}$$

where the decision variable N is a nonnegative integer. For the other models, the corresponding constraints are changed to equation (2.28). In addition, the solar component of the objective function is replaced with the wind component. The objective function of our main model can thus be rewritten as follows:

$$\begin{aligned} \text{minimize } & d_h c_H(S_{U_{max}} + S_{L_{max}}) + d_h c_{PG}(PG_{U_{max}} + PG_{L_{max}}) + d_w c_W N + \\ & dist * d_t c_T T_{max} + \frac{\mu}{\Omega}\sum_{\omega=1}^{\Omega}\sum_{t=1}^{T} Z^{t\omega}. \end{aligned}$$

2.3 Numerical Experiments

We present a case study to examine the optimal sizing decisions of a hybrid energy system that can meet a peak demand of 1 GW in the Mediterranean region of Türkiye. This demand is met by solar/wind energy and hydro energy, which is generated by utilizing the water available from the Manavgat river [29]. The solar radiation and wind speed data is obtained for the same region from Homer Energy [30]. The excess solar/wind energy is stored in the PHES facilities, except for the conventional case with no storage option. We take into account the unpredictability of streamflow rate by incorporating the historical data of the previous 19 years into our models for the open-loop PHES facilities and conventional hydropower stations. We note that the closed-loop PHES facilities have no natural water inflow and thus involve no uncertainty.

Table 2.4: Parameters values for numerical experiments.

Unit cost of reservoir	$3/$m^3$
Unit cost of generator	$500/kW
Unit cost of solar panels	$200/$m^2$
Unit cost of wind turbines	$1.7M
Unit cost of diesel	$0.25/kWh
Cost of transmission line	$1.1M/GW
One-sided efficiency of the hydroelectric system	88%
Efficiency of solar panels	12%
Discount factor	5%
Loss in transmission lines	5%
Height of the upper reservoir	100 meters
Height of the lower reservoir	100 meters
Lifetime of solar panels	30 years
Lifetime of the hydroelectric system	60 years
Lifetime of transmission lines	40 years
Lifetime of wind turbines	20 years

The cost, efficiency, and lifetime parameters of the solar farm are obtained from [26] and are presented in Table 2.4. The unit cost of a wind turbine with 900 kW power capacity is assumed to be $1.7M and its lifetime is assumed to be 20 years [31, 32]. The distance between the hydroelectric system and the demand points is assumed to be 50 km. The DOcplex module of Python 3.9.7 was used to solve our models at a workplace with a 2.4GHz Intel Xeon E5-2630 v3 CPU and 64GB RAM.

2.3.1 Analysis of systems with solar farms

We consider the systems with on-stream PHES separately from the systems with closed-loop PHES, seawater-PHES, and conventional hydropower stations. We present and discuss our results for these two groups in the following two subsections, respectively.

2.3.1.1 Systems with open-loop PHES

For our analysis, we assume that the amount of streamflow entering the system remains the same across different PHES configurations. When there is water inflow to both reservoirs, half of the streamflow feeds the upper reservoir and the other half feeds the lower reservoir. The optimal sizing decisions for the open-loop PHES systems are shown in Table 2.5.

The best open-loop system in terms of *expected* cost is the case when the water flows only into the upper reservoir. All component sizes in this case are smaller than those in the other cases. This is because the PHES reservoirs are used to store energy via water pumped, and the need for storage and pumping (and thus large reservoirs) is lower with water entering the system through the upper reservoir. We observe that the *expected* system costs decline as the component sizes decrease. However, the systems with smaller components benefit less from the renewable sources, leading to higher mismatched demand. We also observe an increase in curtailed solar energy as the component sizes decrease. This situation is another outcome of pumping less: the incoming solar energy tends to be curtailed if it is not used to pump water in the PHES facility.

The expected percentage contributions of renewable sources to meet the demand for open-loop PHES systems are presented in Figure 2.5a. The mismatched demand is below 8% for all open-loop PHES systems. When the water flows only into the lower reservoir, the mismatched demand is at its minimum, and there is slightly more reliance on hydro than the other two configurations. These results can be explained by the larger system components and increased pumping capability in this case. The hydro and solar contributions are 49% and 46%, respectively, in this case. When the water flows only into the upper reservoir, the hydro and solar contributions are 47% and 45%, respectively. When the water flows into both reservoirs, the hydro and solar contributions are 48% and 45%, respectively.

The expected utilized amounts of solar energy in pumping water and meeting

Table 2.5: Comparison of systems with open-loop PHES and solar farms.

Water inflow to	Upper reservoir	Lower reservoir	Both reservoirs
Upper res. cap. (km^3)	0.146	0.365	0.229
Lower res. cap. (km^3)	0.038	0.053	0.040
Upper gen. cap. (GW)	1.404	1.556	1.468
Lower gen. cap. (GW)	0.145	0.239	0.182
Solar panel area (km^2)	23.293	25.610	24.343
Transimssion line cap. (GW)	1.478	1.638	1.545

Expected solar utilization	GWh	%	GWh	%	GWh	%
Directly used solar	2134	42%	2195	39%	2168	41%
Pumped solar	1900	37%	2602	46%	2224	42%
Curtailed solar	1061	21%	806	14%	933	18%
Total solar produced	5096	100%	5603	100%	5326	100%

Expected energy generation	GWh	%	GWh	%	GWh	%
Upper hydro	1805	38%	1861	39%	1811	38%
Lower hydro	457	10%	502	11%	479	10%
Solar	2134	45%	2195	46%	2168	45%
Mismatched demand	380	8%	217	5%	317	7%
Total consumption	4775	100%	4775	100%	4775	100%

Expected system cost ($/kWh)	0.099	0.106	0.102

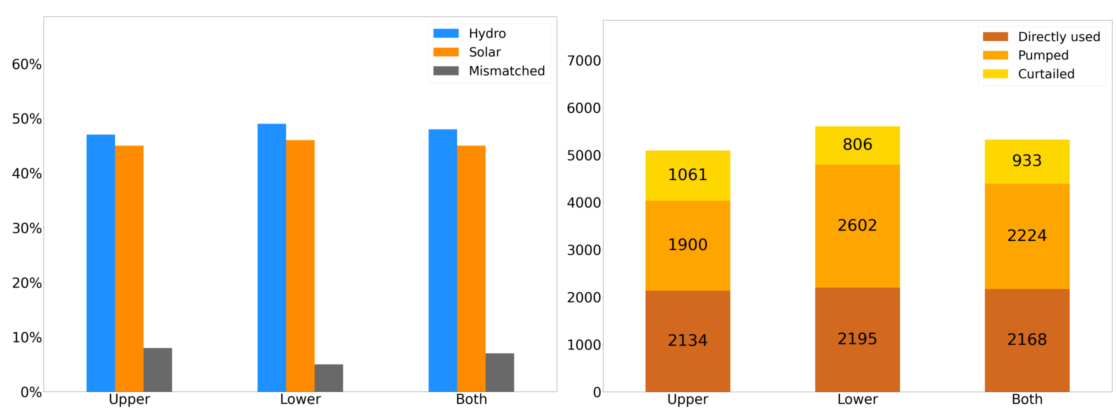

(a) Percentage contributions of resources (b) Solar energy utilization in GWh

Figure 2.5: Comparison of systems with open-loop PHES and solar farms based on renewable energy contribution and solar energy utilization.

demand directly, respectively, are shown in Figure 2.5b. The solar energy produced is lowest, with a total of 5096 GWh, when the water flows only into the upper reservoir. In this case, 46% of the solar energy generated is used to pump water, 41% is used to meet demand directly, and the remaining 13% is curtailed. The solar energy produced is highest, with a total of 5603 GWh, when the water flows only into the lower reservoir. In this case, nearly 50% of the solar energy generated is used to pump water, 38% is used to meet demand directly, and 11% is curtailed. When the water flows into both reservoirs, 48% is used to pump water, 40% is used to meet demand directly, and 12% is curtailed.

2.3.1.2 Systems with closed-loop PHES, seawater-PHES, and conventional hydropower stations

The optimal sizing decisions for the closed-loop PHES systems, seawater-PHES systems, and conventional hydropower stations are shown in Table 2.6. We observe that the closed-loop PHES and seawater-PHES systems outperform the conventional hydropower stations in terms of expected cost. This is because the former two configurations have the energy storage capability while the conventional one does not. The closed-loop PHES and seawater-PHES systems also perform better in meeting demand from renewable resources, highlighting the importance of energy storage in renewable energy systems. The conventional hydropower station has a remarkably small upper reservoir capacity. This is because the system components incur high installation costs so that building a large upper reservoir is not beneficial if it is to be used purely as a generator with no storage option.

Figure 2.6a shows that the expected percentage contributions of renewable sources to meet the demand are similar in the closed-loop PHES and seawater-PHES systems. The storage flexibility provided by the PHES configurations reduce the mismatched demand dramatically. While the mismatched demand is no larger than 13% for all of the PHES configurations, it is 52% for the conventional hydropower station. In our experiments the streamflow rate is the same in all system configurations. However, the hydro contribution is greater than

40% for all of the PHES configurations, but it is less than 10% for the conventional hydropower station. This result implies that the PHES systems utilize the available water inflow much more effectively than the conventional hydropower station. This result is expected since the solar energy cannot be stored in the conventional hydropower station. Figure 6b shows that the amount of solar energy produced in the conventional case is less than half of that in the other two configurations.

The open-loop PHES configurations have lower expected costs than the other PHES configurations. The upper reservoir capacities of open-loop configurations are much higher than those of the other configurations. Although the seawater-PHES system has no lower reservoir and thus has a distinct advantage in terms of installation costs, its upper reservoir capacity is less than that of the open-loop PHES systems. The closed-loop PHES and seawater-PHES systems (with no lower generator) have slightly higher upper generator capacities than the open-loop PHES systems. Since the closed-loop PHES and seawater-PHES systems generate less energy than the open-loop PHES systems, they require installation of wider solar panel areas, inducing larger amounts of solar energy produced. While the amounts of solar energy used to meet demand directly are not very different, the closed-loop PHES and seawater-PHES systems pump more water than the other systems. Although the seawater-PHES system has an access to unlimited amount of water, it has a slightly lower expected cost than the closed-loop PHES system and the amount of water pumped in the seawater-PHES system is only slightly greater than in the closed-loop PHES system.

2.3.2 Analysis of systems with wind farms

We rerun our numerical experiments by replacing the solar component of our hybrid energy system with the wind component. We present our results in the following two subsections.

Table 2.6: Comparison of closed-loop PHES systems, seawater-PHES systems, and conventional hydropower stations, all with solar farms.

System type	Closed-loop		Seawater		Conventional	
Upper res. cap. (km^3)	0.061		0.119		0.007	
Lower res. cap. (km^3)	0.061		-		-	
Upper gen. cap. (GW)	1.570		1.665		0.278	
Lower gen. cap. (GW)	-		-		-	
Solar panel area (km^2)	26.579		27.397		11.611	
Transmission line cap. (GW)	1.652		1.753		0.278	
Expected solar utilization	**GWh**	**%**	**GWh**	**%**	**GWh**	**%**
Directly used solar	2018	35%	2171	36%	1863	73%
Pumped solar	3044	52%	3174	53%	0	0%
Curtailed solar	753	13%	648	11%	677	27%
Total solar produced	5815	100%	5994	100%	2540	100%
Expected energy generation	**GWh**	**%**	**GWh**	**%**	**GWh**	**%**
Hydro	2135	42%	2084	44%	450	9%
Solar	2018	45%	2171	45%	1863	39%
Mismatched demand	622	13%	520	11%	2461	52%
Total consumption	4775	100%	4775	100%	4775	100%
Expected system cost ($/kWh)	0.119		0.116		0.162	

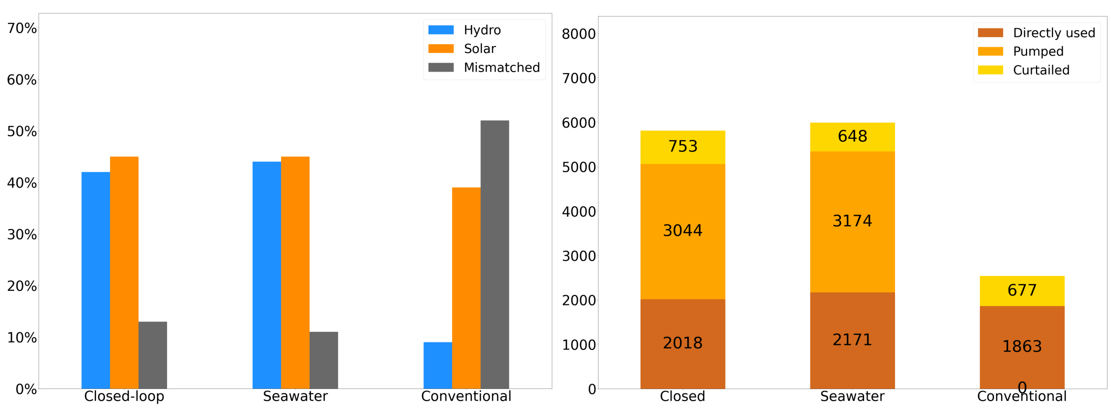

(a) Percentage contributions of resources (b) Solar energy utilization in GWh

Figure 2.6: Comparison of closed-loop PHES systems, seawater-PHES systems, and conventional hydropower stations based on renewable energy contribution and solar energy utilization.

2.3.2.1 Systems with open-loop PHES

We again assume that the amount of streamflow entering the system remains the same across different PHES configurations. When there is water inflow to both reservoirs, half of the streamflow feeds the upper reservoir and the other half feeds the lower reservoir. The optimal sizing decisions for the open-loop PHES systems are shown in Table 2.7.

Similar to the systems with solar farms, the expected system cost and component sizes are lowest when the water flows only into the upper reservoir. However, the sizing decisions of different components are closer here than in the systems with solar farms. Figure 2.7a shows that the wind farm is the major source of energy, followed by the hydropower station, in all three PHES configurations. Figures 2.5b and 2.7b indicate that the amounts of wind energy used to meet demand directly here are larger than the amounts of solar energy used to meed demand directly in the case with solar farms. The amounts of wind energy used to pump water here are smaller than the amounts of solar energy used to pump water in the case with solar farms. These results can be explained by varying levels of availability of renewable resources during the day. While the wind can be available throughout the day, the solar is available only during the daytime. The solar energy should be stored during the daytime if it is to be utilized during the night. Since the solar energy is stored more, the reservoir capacities and the amounts of water pumped are larger in the case with solar farms.

2.3.2.2 Systems with closed-loop PHES, seawater-PHES, and conventional hydropower stations

The optimal sizing decisions for the closed-loop PHES systems, seawater-PHES systems, and conventional hydropower stations are shown in Table 2.8. Figure 2.8a shows that the wind farm is again the major source of energy in all these systems. Figures 6b and 8b indicate that the amounts of wind energy used to meet demand directly here are larger than the amounts of solar energy used to meed demand directly in the case with solar farms. The amounts of wind energy used to pump water here are smaller than the amounts of solar energy used to pump water in the case with solar farms. For the closed-loop PHES and seawater-PHES systems, the mismatched demand here is higher than in the case with solar farms. This is because the solar energy is stored more than the wind energy, and the stored renewable energy helps reduce the mismatched demand more effectively. Finally, the seawater-PHES systems experience very little curtailment of wind energy.

Table 2.7: Comparison of systems with open-loop PHES and wind farms.

Water inflow to	Upper reservoir		Lower reservoir		Both reservoirs	
Upper res. cap. (km^3)	0.065		0.075		0.070	
Lower res. cap. (km^3)	0.057		0.067		0.063	
Upper gen. cap. (GW)	0.960		1.128		1.057	
Lower gen. cap. (GW)	0.143		0.173		0.157	
Number of wind turbines	2569		2869		2740	
Transmission line cap. (GW)	1.010		1.188		1.112	
Expected wind utilization	**GWh**	**%**	**GWh**	**%**	**GWh**	**%**
Directly used wind	2379	59%	2543	57%	2489	58%
Pumped wind	740	18%	1195	27%	947	22%
Curtailed wind	898	22%	748	17%	848	20%
Total wind produced	4017	100%	4486	100%	4284	100%
Expected energy generation	**GWh**	**%**	**GWh**	**%**	**GWh**	**%**
Upper hydro	982	21%	844	18%	899	19%
Lower hydro	436	9%	455	9%	447	9%
Wind	2379	50%	2543	53%	2489	52%
Mismatched demand	987	21%	933	20%	939	20%
Total consumption	4775	100%	4775	100%	4775	100%
Expected system cost (\$/kWh)	0.135		0.144		0.139	

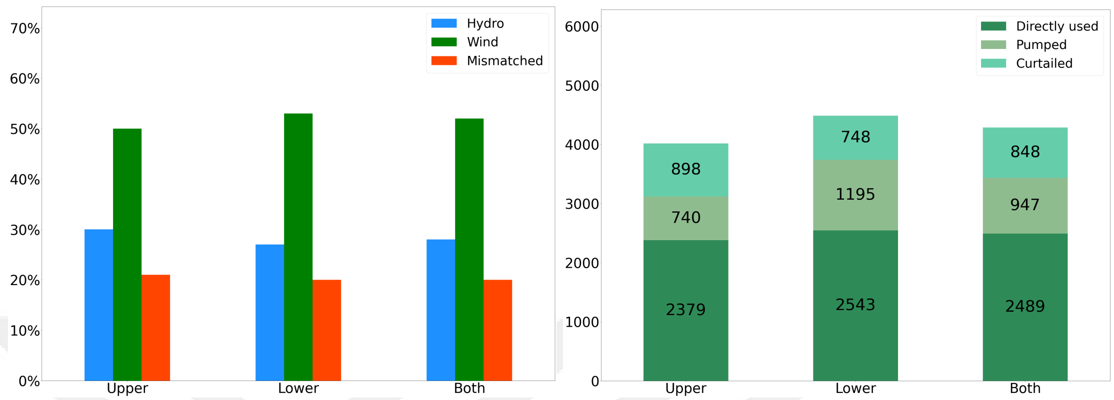

(a) Percentage contributions of resources (b) Wind energy utilization in GWh

Figure 2.7: Comparison of systems with open-loop PHES and wind farms based on renewable energy contribution and wind energy utilization.

Table 2.8: Comparison of closed-loop PHES systems, seawater-PHES systems, and conventional hydropower stations, all with wind farms.

System type	Closed-loop		Seawater		Conventional	
Upper res. cap. (km^3)	0.105		0.142		0.008	
Lower res. cap. (km^3)	0.105		-		-	
Upper gen. cap. (GW)	1.435		1.449		0.156	
Lower gen. cap. (GW)	-		-		-	
Number of wind turbines	3395		3390		2040	
Transmission line cap. (GW)	1.510		1.526		0.156	
Expected wind utilization	GWh	%	GWh	%	GWh	%
Directly used wind	2491	47%	2601	49%	2225	70%
Pumped wind	2076	39%	2430	46%	0	0%
Curtailed wind	741	14%	270	5%	965	30%
Total wind produced	5308	100%	5300	100%	3190	100%
Expected energy generation	GWh	%	GWh	%	GWh	%
Hydro	1463	31%	1386	29%	221	5%
Wind	2491	52%	2601	55%	2252	47%
Mismatched demand	820	17%	787	17%	2328	49%
Total consumption	4775	100%	4775	100%	4775	100%
Expected system cost ($/kWh)	0.156		0.152		0.181	

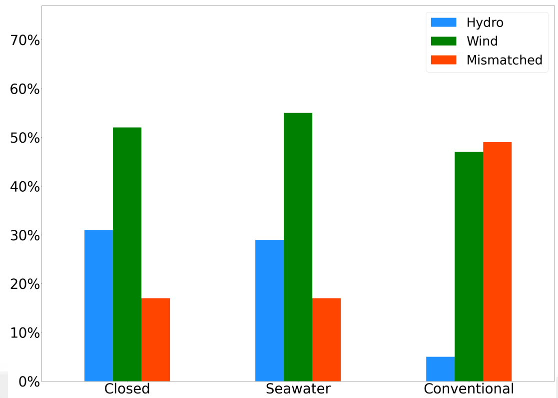

(a) Percentage contributions of resources

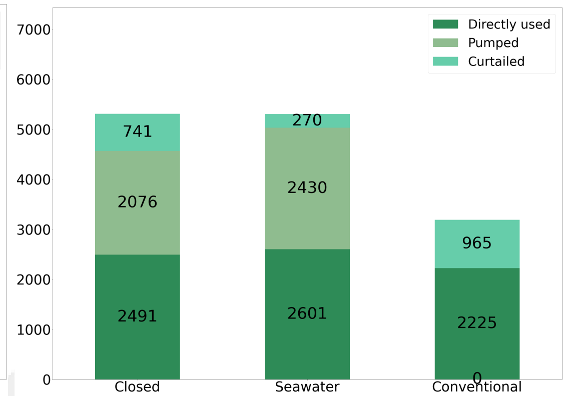

(b) Wind energy utilization in GWh

Figure 2.8: Comparison of closed-loop PHES systems, seawater-PHES systems, and conventional hydropower stations based on renewable energy contribution and wind energy utilization.

2.3.3 The impact of hydropower uncertainty

Two main indicators for assessing the importance of solving our two-stage stochastic programming models (for the open-loop PHES configurations) are the Expected Value of Perfect Information (EVPI) and the Value of Stochastic Solution (VSS). Our computations of EVPI and VSS are based on the methods described in [33]. We refer to the problem given in Section 2.2.2 by equations (2.5)–(2.8) as the recourse problem. We compute EVPI by solving a deterministic problem for each scenario individually, averaging the optimal cost values of all these problems to obtain the *wait-and-see* solution (WS), and comparing it with the optimal cost of the recourse problem (RP). Specifically, let G_ω denote the optimal cost of the following deterministic problem for scenario ω:

$$
\begin{aligned}
\min\ & c^T x + d_\omega^T y_\omega \\
\text{s.t.}\ & Ax = b, \\
& T_\omega x + W_\omega y_\omega = h_\omega, \\
& x \geq 0,\ y_\omega \geq 0.
\end{aligned}
$$

Hence WS $= \frac{\sum_{\omega=1}^{\Omega} G_\omega}{\Omega}$ and EVPI = RP − WS. EVPI represents the maximum amount of money that one would be willing to pay to obtain perfect information about the future streamflow rates. For computation of VSS, we first calculate the scenario $\bar{\omega}$ by averaging all available scenarios in the recourse problem. We then solve the following deterministic problem for scenario $\bar{\omega}$:

$$
\begin{aligned}
\min\ & c^T x + d_{\bar{\omega}}^T y_{\bar{\omega}} \\
\text{s.t. } & Ax = b, \\
& T_{\bar{\omega}} x + W_{\bar{\omega}} y_{\bar{\omega}} = h_{\bar{\omega}}, \\
& x \geq 0,\ y_{\bar{\omega}} \geq 0.
\end{aligned}
$$

We refer to the solution of the above problem as the *expected value solution* and denote by $\bar{x}$ its first-stage decisions. We next implement these first-stage decisions into the recourse problem as follows:

$$
\begin{aligned}
\min\ & c^T \bar{x} + \sum_{\omega} p_\omega d_\omega^T y_\omega \\
\text{s.t. } & A\bar{x} = b, \\
& T_\omega \bar{x} + W_\omega y_\omega = h_\omega \quad \forall \omega, \\
& y_\omega \geq 0 \quad \forall \omega.
\end{aligned}
$$

The optimal cost of the above problem yields the expected result of taking the first-stage decisions of the expected value solution and the optimal second-stage decisions (conditional on the first-stage decisions). We obtain VSS by comparing this expected result (EEV) with the optimal cost of the recourse problem: VSS = EEV − RP. Tables 2.9 and 2.10 exhibit the EVPI and VSS values for the open-loop PHES systems with solar farms and wind farms, respectively. Tables 2.9 and 2.10 also show the EVPI and VSS percentages that are calculated as $\frac{EVPI}{RC} \times 100$

and $\frac{VSS}{RC} \times 100$, respectively.

We observe that the EVPI and VSS percentages are larger in the case with solar farms than in the case with wind farms in general. These results can be explained by the higher degree of intermittency of solar radiation and the resulting lower flexibility in handling uncertainty. An exception to this observation arises in the VSS percentage when the system has a solar farm and the water flows only into the upper reservoir. This result implies that the first-stage decisions (i.e., the sizing decisions) of the expected value solution are similar to the optimal first-stage decisions of the stochastic model, leading to a smaller VSS percentage in this specific case.

Table 2.9: EVPI and VSS values for systems with open-loop PHES and solar farms.

Cost ($) / Water inflow	Upper	Lower	Both
RP	472,787,413	506,300,297	486,983,828
WS	468,418,476	503,617,172	483,311,016
EVPI	4,368,937	2,683,125	3,672,812
% EVPI	**0.92%**	**0.53%**	**0.75%**
EEV	474,482,019	516,157,139	491,208,620
VSS	1,694,606	9,856,842	4,224,791
% VSS	**0.36%**	**1.95%**	**0.87%**

Table 2.10: EVPI and VSS values for systems with open-loop PHES and wind farms.

Cost ($) / Water inflow	Upper	Lower	Both
RP	646,432,892	685,287,407	665,147,628
WS	645,406,104	684,022,405	662,753,772
EVPI	1,026,788	1,265,002	2,393,856
% EVPI	**0.16%**	**0.18%**	**0.36%**
EEV	651,941,889	686,329,963	668,805,385
VSS	5,508,998	1,042,557	3,657,756
% VSS	**0.85** %	**0.15**%	**0.55**%

2.4 Sensitivity Analysis

We performed sensitivity analysis by changing the unit cost of diesel (that we use as a proxy for the cost of backup source) and the unit installation costs of solar/wind farms. The results are shown in Tables 2.11-2.14. The "base case" columns of all these tables correspond to our results in Section 2.3. The upper panels of all these tables show how the optimal sizing decisions vary when we double the unit cost of diesel (μ) or halve it. The lower panels of Tables 2.11 and 2.12 show how the optimal sizing decisions vary when we double the unit installation cost of solar farm (c_S) or halve it. The lower panels of Tables 2.13 and 2.14 show how the optimal sizing decisions vary when we double the unit installation cost of wind farm (c_W) or halve it.

As expected, the optimal sizes of solar/wind farms grow as the diesel cost increases or as the installation costs decrease. For the systems with open-loop PHES and solar farms, the upper reservoir/generator capacity is more sensitive to changes in the diesel and solar installation costs, in comparison with the lower reservoir/generator capacity. The cost changes have a larger impact on the upper reservoir capacity of the seawater-PHES system than on those of the closed-loop PHES system and the conventional hydropower station. This result can be attributed to the larger upper reservoir of seawater-PHES system in general. For the systems with open-loop PHES and wind farms, the upper reservoir/generator capacity is more sensitive to changes in the diesel cost (but not in the wind installation cost), in comparison with the lower reservoir/generator capacity. The cost changes again have a greater impact on the upper reservoir capacity of the seawater-PHES system than on those of the closed-loop PHES system and the conventional hydropower station.

Table 2.11: Sensitivity analysis for open-loop PHES systems with solar farms.

	Diesel cost x 2			Base case			Diesel cost / 2		
Water inflow to	Upper	Lower	Both	Upper	Lower	Both	Upper	Lower	Both
Upper. res. cap. (km^3)	0.499	0.542	0.517	0.146	0.365	0.229	0.026	0.027	0.025
Lower res. cap. (km^3)	0.063	0.071	0.066	0.038	0.053	0.040	0.017	0.023	0.020
Upper gen. cap. (GW)	1.557	1.608	1.587	1.404	1.556	1.468	0.609	0.844	0.718
Lower gen. cap. (GW)	0.139	0.205	0.171	0.145	0.239	0.182	0.165	0.203	0.186
Solar panel area (km^2)	25.632	27.145	26.298	23.293	25.610	24.343	13.466	16.211	14.726
Trans. line cap. (GW)	1.639	1.693	1.671	1.478	1.638	1.545	0.641	0.889	0.756
	Solar cost x 2			**Base case**			**Solar cost / 2**		
Water inflow to	Upper	Lower	Both	Upper	Lower	Both	Upper	Lower	Both
Upper. res. cap. (km^3)	0.087	0.109	0.075	0.146	0.365	0.229	0.099	0.237	0.099
Lower res. cap. (km^3)	0.024	0.029	0.026	0.038	0.053	0.040	0.058	0.062	0.060
Upper gen. cap. (GW)	0.873	1.114	0.958	1.404	1.556	1.468	1.404	1.453	1.420
Lower gen. cap. (GW)	0.175	0.221	0.209	0.145	0.239	0.182	0.130	0.223	0.161
Solar panel area (km^2)	15.197	17.822	16.212	23.293	25.610	24.343	28.151	29.605	28.726
Trans. line cap. (GW)	0.919	1.172	1.009	1.478	1.638	1.545	1.478	1.530	1.495

Table 2.12: Sensitivity analysis for other systems with solar farms.

	Diesel cost x 2			Base case			Diesel cost / 2		
System type	Closed	Seawater	Conv.	Closed	Seawater	Conv.	Closed	Seawater	Conv.
Upper. res. cap. (km^3)	0.084	1.191	0.019	0.061	0.119	0.007	0.029	0.034	0.005
Lower res. cap. (km^3)	0.084	-	-	0.061	-	-	0.029	-	-
Upper gen. cap. (GW)	1.688	1.574	0.332	1.570	1.665	0.278	1.030	1.031	0.220
Lower gen. cap. (GW)	-	-	-	-	-	-	-	-	-
Solar panel area (km^2)	31.684	29.703	16.628	26.579	27.397	11.611	18.347	18.238	8.336
Trans. line cap. (GW)	1.777	1.657	0.332	1.652	1.753	0.278	1.084	1.085	0.220
	Solar cost x 2			**Base case**			**Solar cost / 2**		
System type	Closed	Seawater	Conv.	Closed	Seawater	Conv.	Closed	Seawater	Conv.
Upper. res. cap. (km^3)	0.051	0.063	0.006	0.061	0.119	0.007	0.062	0.093	0.008
Lower res. cap. (km^3)	0.051	-	-	0.061	-	-	0.062	-	-
Upper gen. cap. (GW)	1.387	1.408	0.266	1.570	1.665	0.278	1.523	1.548	0.297
Lower gen. cap. (GW)	-	-	-	-	-	-	-	-	-
Solar panel area (km^2)	20.694	20.836	8.380	26.579	27.397	11.611	32.342	32.157	16.587
Trans. line cap. (GW)	1.460	1.482	0.266	1.652	1.753	0.278	1.603	1.629	0.297

Table 2.13: Sensitivity analysis for open-loop PHES systems with wind farms.

	Diesel cost x 2			Base case			Diesel cost / 2		
Water inflow to	Upper	Lower	Both	Upper	Lower	Both	Upper	Lower	Both
Upper. res. cap. (km^3)	1.016	0.931	0.987	0.065	0.075	0.070	0.021	0.014	0.017
Lower res. cap. (km^3)	0.110	0.130	0.122	0.057	0.067	0.063	0.008	0.010	0.008
Upper gen. cap. (GW)	1.424	1.627	1.517	0.960	1.128	1.057	0.274	0.319	0.255
Lower gen. cap. (GW)	0.164	0.180	0.169	0.143	0.173	0.157	0.176	0.206	0.189
# wind turbines	3490	3854	3654	2569	2869	2740	1101	1283	1177
Trans. line cap. (GW)	1.499	1.712	1.596	1.010	1.188	1.112	0.450	0.363	0.444
	Wind cost x 2			**Base case**			**Wind cost / 2**		
Water inflow to	Upper	Lower	Both	Upper	Lower	Both	Upper	Lower	Both
Upper. res. cap. (km^3)	0.059	0.040	0.041	0.065	0.075	0.070	0.071	0.085	0.076
Lower res. cap. (km^3)	0.015	0.023	0.019	0.057	0.067	0.063	0.065	0.075	0.069
Upper gen. cap. (GW)	0.379	0.615	0.490	0.960	1.128	1.057	1.294	1.467	1.375
Lower gen. cap. (GW)	0.175	0.232	0.203	0.143	0.173	0.157	0.102	0.112	0.108
# wind tubines	1200	1551	1369	2569	2869	2740	4048	4425	4236
Trans. line cap. (GW)	0.554	0.648	0.557	1.010	1.188	1.112	1.363	1.544	1.447

Table 2.14: Sensitivity analysis for other systems with wind farms.

	Diesel cost x 2			**Base case**			**Diesel cost / 2**		
System type	Closed	Sewater	Conv.	Closed	Sewater	Conv.	Closed	Sewater	Conv.
Upper. res. cap. (km^3)	0.149	0.224	0.025	0.105	0.142	0.008	0.009	0.015	0.002
Lower res. cap. (km^3)	0.149	-	-	0.105	-	-	0.009	-	-
Upper gen. cap. (GW)	2.230	2.169	0.230	1.435	1.449	0.156	0.271	0.391	0.105
Lower gen. cap. (GW)	-	-	-	-	-	-	-	-	-
# wind turbines	4845	4707	3665	3395	3390	2040	1266	1408	944
Trans. line cap. (GW)	2.347	2.283	0.230	1.010	1.526	0.156	0.285	0.411	0.105
	Wind cost x 2			**Base case**			**Wind cost / 2**		
System type	Closed	Sewater	Conv.	Closed	Sewater	Conv.	Closed	Sewater	Conv.
Upper. res. cap. (km^3)	0.029	0.055	0.004	0.105	0.142	0.008	0.096	0.145	0.013
Lower res. cap. (km^3)	0.029	-	-	0.105	-	-	0.096	-	-
Upper gen. cap. (GW)	0.722	0.883	0.138	1.435	1.449	0.156	1.546	1.773	0.183
Lower gen. cap. (GW)	-	-	-	-	-	-	-	-	-
# wind turbines	1714	1907	948	3395	3390	2040	4708	4975	3653
Trans. line cap. (GW)	0.760	0.929	0.138	1.010	1.526	0.156	1.628	1.867	0.183

2.5 Conclusion

In this chapter, we present two-stage stochastic mixed-integer programming models for various PHES configurations and investigate how the choice of PHES configuration impacts the sizing decisions of hybrid energy systems with solar/wind farms. We conduct numerical experiments by utilizing the real historical data of streamflow rates to generate the scenarios of our stochastic programming models. Our results show that the PHES systems can significantly reduce the need for fossil fuels in both cases of solar and wind farms. The open-loop PHES configurations perform better than the other PHES configurations in terms of expected system costs. For the open-loop PHES systems, the system cost is lowest when the water flows only into the upper reservoir.

This chapter and its results may lead to many different studies in the future. In order to reflect the real-life situations better, the uncertainties not only in the streamflow rate but also in the other renewable sources might be jointly incorporated into stochastic programming models. Such an extension will likely require a larger number of scenarios, leading to large-scale problems that are computationally challenging. Such problems may be solved by developing and using decomposition-based solution techniques such as L-shaped method [29]. Future research may also consider jointly optimizing the sizing and operational decisions via multi-stage stochastic programming models. Lastly, future work may look into the environmental and social aspects of the sizing and operational decisions.

Chapter 3

MDP Formulation for Operational Planning of a Decentralized Wind Farm

3.1 Introduction

For the past decades, the worldwide energy demand has grown rapidly, leading to a significant depletion of fossil fuels for energy generation and causing a rise in greenhouse gas emissions. There has also been a rapid transition to renewable energy sources to address the environmental consequences of fossil-fuel based energy generation. The renewable sources include solar, wind, hydropower, biomass, and geothermal energy, which offer sustainable alternatives to fossil fuels and help meet the growing energy demand.

It is estimated that by 2028 the renewable energy sources will account for over 42% of global electricity generation, and the solar and wind share will double to 25% [34]. However, integrating renewable sources into energy systems can pose reliability challenges due to their variable and intermittent nature. Although this issue can be mitigated by adopting efficient and flexible storage systems

[35], relying on energy storage only is not sufficient to completely solve all issues regarding renewable energy integration. While energy storage is essential for grid flexibility, its use is limited by high costs, variable efficiency, and technological readiness, raising the need for additional approaches to properly address the renewable energy integration issues [36]. Another important challenge here is related to operational flexibility of decentralized systems that hinges on supply and demand balancing to ensure system sufficiency and security [37]. Designing and operating decentralized renewable energy systems optimally is a significant task to overcome these challenges.

In a decentralized grid-connected system, energy is distributed through a main grid to a small area such as mountain, village, or island communities, as in Das and Balakrishnan [38], Goel and Sharma [39], and Razmjoo et al. [40]. There is a vast literature on grid-connected systems. Basit et al. [41] give a review of challenges associated with renewable energy systems with storage option, proposing a simulation-based approach to overcome such challenges. Behabtu et al. [42] provide a review of energy storage technologies, underlining the importance of battery usage to deal with variability inherent in renewable energy systems. Farivar et al. [43] also consider various technologies for energy storage, focusing on battery storage systems and their applications. Rana et al. [44] review five different energy storage technologies, demonstrating their advantages and disadvantages regarding their integration into the power grid. Hojabri et al. [45] provide an overview of control technologies of grid-connected renewable energy systems from a technical point of view.

The literature on decentralized grid-connected renewable energy systems with storage can be classified into two categories: (i) design problem and (ii) operational planning problem. Most of the studies dealing with the design problem consider investment planning and related capacity decisions for renewable energy systems ([38], [46], [47], [48]). There is also a significant body of research that deals with the design problem through case studies of natural islands at various locations ([49], [50], [51], [52], [53]).

There are only several comprehensive literature reviews on operational planing of renewable energy systems. We refer the reader to Ammari et al. [54] and Banos et al. [55] for detailed reviews of optimization techniques applied in this research area. Talari et al. [56] and Psarros and Papathanassiou [57] review the literature for stochastic modeling of renewable energy systems. Thirunavukkarasu et al. [58] analyze various optimization methodologies and artificial intelligence techniques for hybrid renewable energy systems. The MDP approach is yet to be stumbled upon among the mentioned literature on operational planning of renewable energy systems, although MDPs offer precise mathematical formulations by capturing intricate dynamics that are present in the real-world scenarios.

Specifically, MDPs allow the decision-maker to act adaptive by making decisions based on the realized outcomes of uncertainties since the future uncertainties are resolved when the decision-maker moves forward in time [59]. Zhou et al. [60] take an MDP approach to find an optimal policy to manage electricity surpluses under negative prices and battery constraints. Hassler [61] develops heuristic rules for short-term trading of a producer having the option of storage. Salas and Powell [62] design an approximate dynamic programming algorithm and obtain near-optimal control policies for grid-level energy storage. Zhou et al. [63] consider an MDP to analyze the managerial decisions of a remote wind farm co-operated with a grid-level storage unit. Avci et al. [64] characterize the optimal policy structure for the energy generation and storage problem of a hybrid energy system consisting of a wind farm and a PHES facility. Toufani et al. [16] use an MDP framework to compare the short-term cash flows of several different PHES configurations. In another work, Toufani et al. [17] use again an MDP framework to study the problem of transforming an existing cascading hydropower station into a PHES facility. Yang et al. [65] use pathwise optimization for merchant energy production. Karakoyun et al. [59] formulate an MDP to study the energy commitment, generation and storage problem of wind power producers.

We consider a decentralized system that is similar to the setting proposed in [63] where the market operations of a wind farm and a battery are jointly optimized. However, our setting involves a small community in a decentralized grid-connected area that wishes to invest in renewable energy generation to fulfill its local energy demand. Therefore, the priority of the system operator is demand fulfillment. The system operator can sell excess available energy to the market or can purchase energy from the market. Considering wind speed, electricity price, and demand uncertainties, we formulate the system operator's real-time energy generation and storage problem as an MDP. We incorporate the time series data for wind speed, electricity price, and demand available for the State of New York into our MDP and solve the problem with backward dynamic programming algorithm. We conduct numerical experiments by considering various realistic configurations of our setting to look into how the capacity levels of system components impact the operational decisions.

We contribute to the literature by considering uncertainties in all system inputs (electricity price, wind speed, and demand) for more effective decision-making for decentralized grid-connected renewable energy systems with demand-fulfillment obligation and energy-storage option. We solve the operational planning problem of the system operator to find the optimal real-time decisions in each period. The problem is solved via hourly periods over a seven-day planning horizon, resulting in weekly operational decisions for the system operator. With the results obtained from this study, we offer managerial insights into both operational and design decisions. To our knowledge, this work is the first in the literature to combine the setting of uncertain price, wind, and demand with the MDP methodology to solve the operational planning problem of the system operator with demand-fulfillment obligation.

The rest of this chapter is organized as follows: Section 3.2 describes the setting consisting of a wind farm and a battery and models the operational planning problem as an MDP. Section 3.3 presents the numerical results for various component sizes. Section 3.4 investigates the impact of several major changes in the problem setting. Section 3.5 examines the effect of considering uncertainties in decision-making on cash flows, and finally, Section 3.6 concludes.

3.2 Problem Formulation

3.2.1 Problem Setting

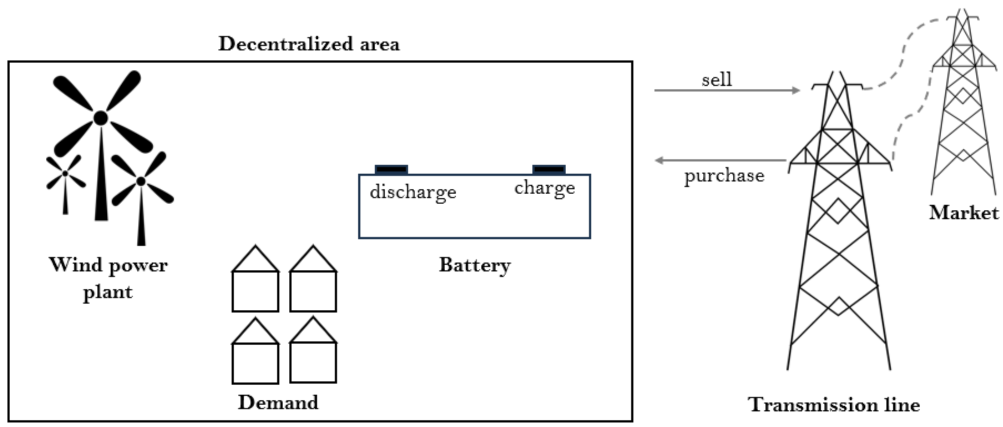

Figure 3.1: Illustration of a decentralized grid-connected wind farm with battery.

The decentralized grid-connected energy system that we consider is illustrated in Figure 3.1. The system operator is primarily obliged to fulfill the decentralized-area demand. The system operator can generate energy from the wind power plant and/or the battery installed to meet the demand. If the available energy is insufficient to meet the demand, the system operator can purchase energy from the market at the market price. If there is excess energy in the system, it is possible to store energy by charging the battery or sell energy to the market to increase revenues. We assume that these purchase/sell decisions do not affect the market prices and that the system operator is a price-taker ([59], [63]). In this setting, we study the energy generation and storage problem over a finite planning horizon of T periods and denote by $\mathscr{T} := \{1, 2..., T\}$ the set of periods. The system operator makes the following decisions in each time period upon resolution of uncertainties in demand, electricity price, and wind speed for the current period:

(i) How much energy to generate from the wind power plant,

(ii) How much energy to generate from the battery by discharging it, and

(iii) How much energy to store in the battery by charging it.

3.2.2 Model Parameters

The battery possesses limited energy and power capacities. Its hourly energy capacity is given by the maximum energy it can store and is denoted by C_S. Its power capacity is the maximum energy it can generate or store within a single period through charging or discharging operations. The power capacities for discharge (generation) and charge (storage) are denoted by K_D and K_C, respectively. The hourly energy capacities for charging and discharging are denoted by $C_C = K_C\Delta t$ and $C_D = K_D\Delta t$, respectively. The term Δt is equal to the length of one time period. The power capacity of the transmission line is also limited and denoted by K_T. Its hourly energy capacity is denoted by $C_T = K_T\Delta t$. The efficiency parameter of the transmission line is $\tau \in (0, 1]$. The efficiency remains the same in both purchasing and selling cases. The efficiency parameters of the battery in discharging and charging cases are $\gamma \in (0, 1]$ and $\theta \in (0, 1]$, respectively.

3.2.3 State Variables

There are four state variables that we consider in our MDP: The amount of energy accumulated in the battery at the beginning of period t is denoted by $S_t \in [0, C_S]$. In any period t, the system operator can sell or purchase energy in a market setting where the electricity price in either case is denoted by P_t ($\in \mathbb{R}$). The effective wind speed in period t is denoted by W_t ($\in \mathbb{R}_+$). The observed decentralized-area demand in period t is denoted by D_t ($\in \mathbb{R}_+$). Finally, our state description involves the tuple $I_t := (P_k, W_k, J_k)_{k \leq t}$ that evolves over time according to an exogenous stochastic process. We include the spike component J_k in tuple I_t following Karakoyun et al. [59]. This tuple allows us to incorporate the time series models constructed for the random system components (i.e., price, wind, and demand) into our MDP.

3.2.4 Decision Variables (Actions)

After observing all state variables (P_t, W_t, D_t, S_t) at the beginning of period t, the system operator determines the amount of energy to generate in the wind farm in period t ($w_t \in \mathbb{R}_+$) and the amount of energy to store or generate in the battery ($s_t \in \mathbb{R}$). The amount of wind energy that can be generated in period t cannot exceed the function $f(W_t)$ that is given by the total number of wind turbines installed in the decentralized area times the energy output of a wind turbine at wind speed W_t.

3.2.5 Transition Functions

The amount of energy accumulated in the battery changes according to the equation $S_{t+1} = S_t - s_t$ from period t to period $t + 1$. The other state variables (P_t, W_t, D_t) are assumed to evolve over time according to different and independent Markovian stochastic processes that are generated from the time series models.

3.2.6 Payoff Function

Assuming non-negative demand ($D_t \geq 0$) and considering the conditions stated above, the system operator can make one of the following decisions:

(i) When the battery is discharged ($s_t \geq 0$) and the available energy is enough to satisfy the demand ($\gamma s_t + w_t - D_t \geq 0$), the excess energy is sold to the market.

(ii) When the battery is discharged ($s_t \geq 0$) and the available energy is not enough to satisfy the demand ($\gamma s_t + w_t - D_t < 0$), the energy required to cover the demand mismatch is purchased from the market.

(iii) When the battery is charged ($s_t < 0$) and the remaining renewable energy is enough to satisfy the demand ($\frac{s_t}{\theta} + w_t - D_t \geq 0$), the excess energy is sold to the market.

(iv) When the battery is charged ($s_t < 0$) and the remaining renewable energy is not enough to satisfy the demand ($\frac{s_t}{\theta} + w_t - D_t < 0$), the energy required to cover the demand mismatch is purchased from the market.

With the above decisions, the energy sold or purchased in period t can be written as:

$$E(s_t, w_t) := \begin{cases} (\gamma s_t + w_t - D_t)\tau & \text{if } s_t \geq 0 \text{ and } \gamma s_t + w_t - D_t \geq 0 \\ (\gamma s_t + w_t - D_t)/\tau & \text{if } s_t \geq 0 \text{ and } \gamma s_t + w_t - D_t < 0 \\ (\frac{s_t}{\theta} + w_t - D_t)\tau & \text{if } s_t < 0 \text{ and } \frac{s_t}{\theta} + w_t - D_t \geq 0 \\ (\frac{s_t}{\theta} + w_t - D_t)/\tau & \text{if } s_t < 0 \text{ and } \frac{s_t}{\theta} + w_t - D_t < 0 \end{cases}$$

Given the state variables in period t (S_t and I_t), $\mathbb{U}(S_t, I_t)$ denotes the set of action pairs $(s_t, w_t) \in R \times R_+$ that satisfy the constraints below:

$$0 \leq w_t \leq f(W_t) \tag{3.1}$$

$$-\min\{C_S - S_t, C_C\} \leq s_t \leq \max\{S_t, C_D\} \tag{3.2}$$

$$-\tau C_T \leq \gamma s_t + w_t - D_t \leq C_T \tag{3.3}$$

$$-\tau C_T \leq \frac{s_t}{\theta} + w_t - D_t \leq C_T \tag{3.4}$$

Equation 3.1 ensures that the wind energy generated in any period has an upper bound $f(W_t)$. Equation 3.2 demonstrates the finite energy and power capacities of the battery that limits its charging and discharging operations. Equations 3.3 and 3.4 correspond to the transmission capacity constraints. If some energy is sold to the market, the amount of energy sold cannot exceed τC_T due to the transmission loss. However, if some energy is purchased from the market, the amount of energy purchased cannot exceed C_T. The market pays for the purchasing cost of the energy it receives on the other end of the transmission line, whereas the system operator pays for the purchasing cost of the energy the market sends from the other end of the transmission line. If the available energy in the system is not sufficient to meet the demand, the energy required to meet the demand must be purchased from the market. Therefore, the transmission line capacity must be at least as high as the mismatched demand to be able to entirely meet the demand. In an extreme case with $s_t = w_t = 0$, the amount of energy that must be purchased to fulfill the demand D_t is $\frac{D_t}{\tau}$. Therefore, we assume that $\frac{D_t}{\tau} \leq C_T$ to ensure demand fulfillment. With these constraints, the payoff function is given by the electricity price in period t multiplied by the energy sold or purchased in period t:

$$R(I_t, s_t, w_t) := P_t E(s_t, w_t). \tag{3.5}$$

3.2.7 Objective Function

We note that $\mathbb{U}(S_t, I_t)$ is set of action pairs (s_t, w_t) that are admissible in state (S_t, I_t). We now define π as the feasible policy that is a sequence of decision rules denoted by $(\eta_t^\pi(S_t, I_t))_{t\in T}$. The sequence $(\eta_t^\pi(S_t, I_t))_{t\in T}$ maps the storage level S_t to the feasible action pair $((s_t^\pi(S_t, I_t)), (w_t^\pi(S_t, I_t)))$ in each period t. We also define Π as the set of all possible feasible policies. Hence, for any initial state (S_1, I_1), the optimal expected total cash flow can be expressed as follows:

$$\max_{\pi\in\Pi} \mathbb{E}\left[\sum_{t\in T} R(I_t, s_t^\pi(S_t^\pi, I_t), w_t^\pi(S_t^\pi, I_t)) \middle| S_1, I_1\right]. \tag{3.6}$$

The above problem can be solved via a dynamic programming recursion. Specifically, the optimal profit function $v_t^*(S_t, I_t)$ for each period $t \in T$ and each state (S_t, I_t) can be calculated as follows:

$$v_t^*(S_t, I_t) := \max_{(s_t, w_t)\in\mathbb{U}(S_t, I_t)} \{R(I_t, s_t, w_t) + \mathbb{E}_{I_{t+1}|I_t}[v_{t+1}^*(S_{t+1}, I_{t+1})]\}. \tag{3.7}$$

We assume $v_T(S_T, I_T) = 0$ in the above recursion. Finally, we note that $v_1^*(S_1, I_1)$ is the optimal expected total cash flow if the initial system state is (S_1, I_1).

3.3 Numerical Experiments

3.3.1 The Experimental Setup and Data

In our experiments, we consider a setting in which the planning horizon is one-week long. This implies that $T = 168$ hours. We run our experiments for the first week of August. We assume that the transmission line efficiency is 0.97 and the battery round-trip efficiency is 0.85 based on previous research (Zhou et al. [63] and Karakoyun et al. [59]). For the electricity price and wind speed, we adopt the time series models that Karakoyun et al. [59] have constructed based on the electricity-price data available for the 2007–2019 period and the wind-speed data available for the 2007–2012 period, both for Albany in the State of New York. The components of the electricity-price model are seasonality (via linear regression), mean reversion (via autoregressive model of order one), and spike (via empirical distribution). The components of the wind-speed model are seasonality (via linear regression with Fourier terms) and mean reversion (via autoregressive model of order one).

For the electricity demand, we consider the data available for the 2021–2023 period for the State of New York [66]. We scale down the demand data based on the size of our decentralized grid-connected power system to obtain realistic results. Specifically, the average, median, minimum, and maximum demand values are reduced to 5.56 MW, 5.41 MW, 3.76 MW, and 10 MW, respectively. We then employ the STL method introduced by Cleveland et al. [67] and embedded into Pyhton's `STL()` function under the `statsmodel` library. The `STL()` function uses a non-parametric regression model called Locally Estimated Scatterplot Smoothing (LOESS). It first estimates the seasonality component through LOESS for each cycle. It then estimates the trend component of the deseasonalized data again through LOESS. Residuals are computed by subtracting the seasonality and trend components from the original data.

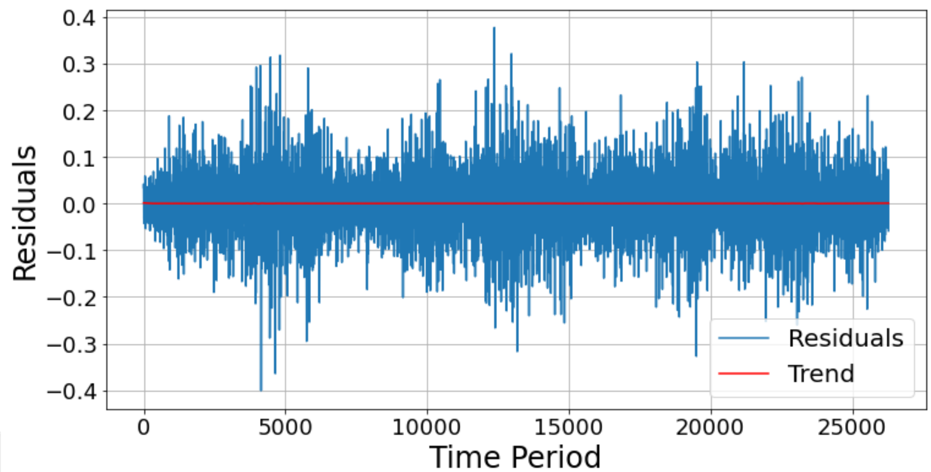

Figure 3.2: Residuals and trend line for the demand data.

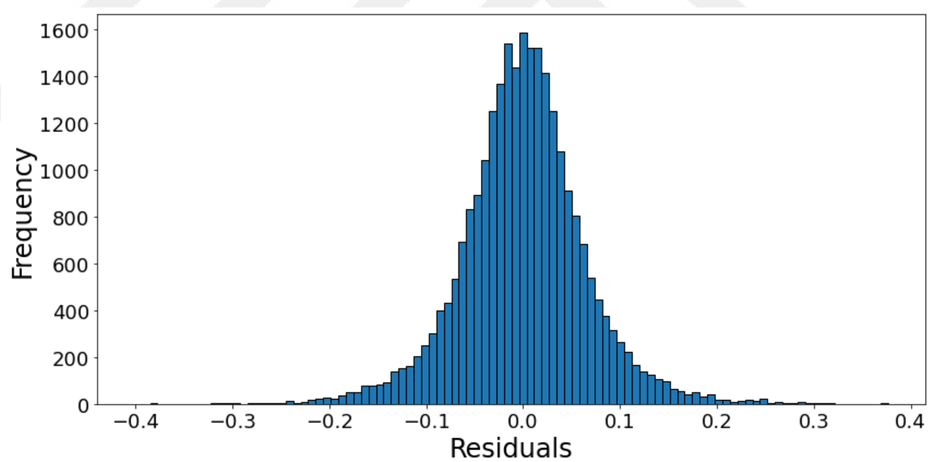

Figure 3.3: Histogram for the deseasonalized demand data.

Table 3.1: Deseasonalized demand values (MWh) and their occurrence probabilities.

Deseasonal Demand	-3.36	-2.06	-0.768	0.528	1.82	3.12
Probability	0.00095	0.02	0.39	0.55	0.03	0.0022

Using STL() in Python, we decompose the demand data by removing the hourly, daily and yearly seasonal components. The values of residuals after removing these seasonality components are shown in Figure 3.2. Since no trend has been observed from the residual plot, the trend component is assumed to be insignificant. The histogram of residuals shown in Figure 3.3 follows a normal-like distribution. We divide the residual data into six discrete levels and embed the resulting discrete distribution into our MDP. The discrete deseasonalized demand data and associated probabilities are shown in Table 3.1, and its histogram is given in Figure 3.4. In each period t, we first compute the deseasonalized demand value according to these probabilities and then add the previously computed hourly, daily, and yearly seasonal components. Fitting the model to the data available for the 2021–2023 period and predicting the demand for the first six months of 2024, we obtain the plots for actual demand values versus predictions that we relegate to Appendix A. We have found that the mean absolute error (MAE) of our predictions is only 0.085 MWh.

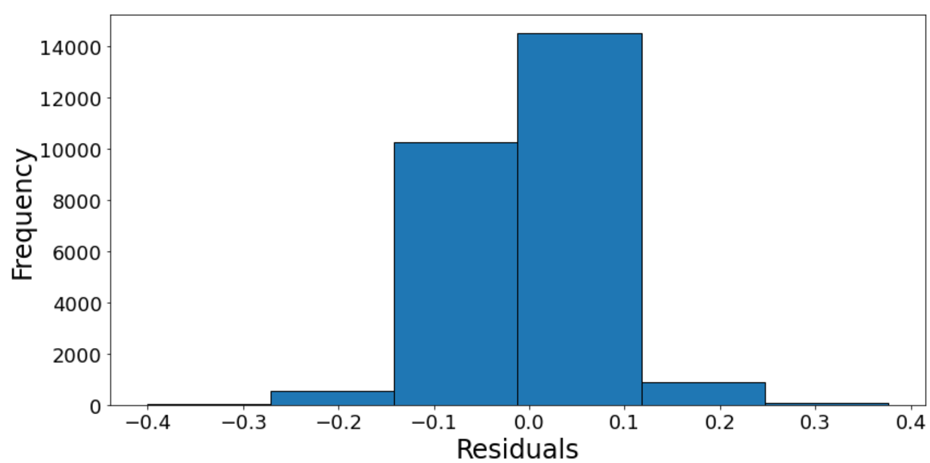

Figure 3.4: Histogram for the discrete deseasonalized demand data.

We determine the capacity levels of system components by ensuring that all demand is met in each period. Hence, the number of GE 1.5(MW)-77 turbines takes values from the set {10, 15, 20}, $C_C = C_D \in \{5, 10\}$ MWh, $C_S \in \{50, 100\}$ MWh, and $C_T \in \{10, 50\}$ MWh. As noted by Karakoyun et al. [59], the negative price frequency is 4.02%. The initial storage level S_1 is the closest state to $C_S/2$ and the initial exogenous state is the closest state to the average level ([59], [64]).

Following the notation of Karakoyun et al. [59], $I_1 := (\xi_1, \rho_1, j_1) = (5, 0, 0)$. We calculate the below metrics by solving the recursion of our MDP to optimality in each instance:

- Expected total cash flow in million dollars (TCF),
- Expected total energy purchased in MWh (EP),
- Expected total energy sold in MWh (ES),
- Expected total renewable energy generation in MWh (RG),
- Expected average battery storage level over all time periods in MWh (BL).

3.3.2 Numerical Results

The numerical results for various capacity levels of system components are given in Table 3.2. The total demand observed in each instance is 1093 MWh and all demand is fulfilled in each period.

Table 3.2: Metric results for different capacity levels of system components.

C_T	C_C=C_D	C_S	n_{trb}	TCF	EP	ES	RG	BL
10	5	50	10	0.030	213	614	1705	26
			15	0.050	91	998	2388	29
			20	0.059	42	1206	2803	31
		100	10	0.031	202	619	1738	47
			15	0.051	73	1021	2436	53
			20	0.061	33	1239	2886	59
	10	50	10	0.035	301	675	1767	27
			15	0.053	140	1032	2438	30
			20	0.062	68	1238	2871	32
		100	10	0.037	331	701	1847	52
			15	0.055	137	1067	2539	56
			20	0.065	55	1291	3016	60
50	5	50	10	0.035	297	634	1700	25
			15	0.070	208	1280	2454	25
			20	0.105	163	1968	3207	25
		100	10	0.037	296	650	1733	45
			15	0.072	209	1297	2486	45
			20	0.107	164	1986	3239	45
	10	50	10	0.043	405	708	1774	26
			15	0.079	284	1321	2533	26
			20	0.114	230	2001	3287	26
		100	10	0.047	493	775	1889	49
			15	0.082	341	1361	2646	50
			20	0.118	274	2027	3400	50

Table 3.2 shows that TCF and RG increase with the transmission line capacity, charge/discharge capacity, storage capacity, and number of turbines. EP and ES increase with the charge/discharge and storage capacities. However, increasing the number of turbines reduces EP but increases ES. BL increases with the charge/discharge and storage capacities but decreases with the transmission line capacity. Our aim in this chapter is to quantify these intuitive observations to gain further insights into the capacity investment choices of the decision-maker. To this end, we will highlight some important results from the table.

Table 3.3 compares the values of TCF when the transmission line capacity or the charge/discharge capacity is increased. The last column of the table shows the percentage TCF improvements thanks to an increment in the transmission line capacity when $C_C = C_D = 10$ MWh. We observe that the percentage TCF improvement is higher when the number of turbines is larger. Table 3.3 also shows the percentage TCF improvements thanks to an increment in the charge/discharge capacity. We observe that the percentage TCF improvement is lower when the number of turbines is larger. With higher transmission line and storage capacities, the percentage TCF improvement is at most 29%. We can observe similar percentage improvements in different settings. For example, the percentage TCF improvement is 8% in the following two settings: $C_S = 100$ MWh and $C_T = 10$ MWh with 15 turbines versus $C_S = 50$ MWh and $C_T = 50$ MWh with 20 turbines.

Table 3.3: Percentage TCF improvements when the transmission line capacity or the charge/discharge capacity is increased.

C_S	n_{trb}	C_T=10			C_T=50			**% impr.**
		C_C=C_D=5	C_C=C_D=10	**% impr.**	C_C=C_D=5	C_C=C_D=10	**% impr.**	(C_C=C_D=10)
50	10	0.030	0.035	16%	0.035	0.043	24%	25%
	15	0.050	0.053	6%	0.070	0.079	12%	49%
	20	0.059	0.062	5%	0.105	0.114	8%	83%
100	10	0.031	0.037	19%	0.037	0.047	29%	27%
	15	0.051	0.055	8%	0.072	0.082	15%	49%
	20	0.061	0.065	7%	0.107	0.118	10%	81%

Table 3.4 compares the values of TCF when the storage capacity or the number of turbines is doubled. The impact of increasing the number of turbines is lowest when $C_C = C_D = 10$ MWh, $C_S = 100$ MWh, and $C_T = 10$ MWh. Increasing the number of turbines has a much greater impact than increasing the battery storage capacity. The percentage TCF improvement thanks to increased storage capacity is higher when the number of turbines is lower. The low number of turbines limits the wind energy generation and the resulting energy scarcity makes the system more sensitive to changes in the capacity levels of other system components.

Table 3.4: Percentage TCF improvements when the storage capacity or the number of turbines is doubled.

C_C=C_D	C_S	$C_T = 10$			$C_T = 50$		
		$n_{trb} = 10$	$n_{trb} = 20$	**% impr.**	$n_{trb} = 10$	$n_{trb} = 20$	**% impr.**
5	50	0.030	0.059	99%	0.035	0.105	201%
	100	0.031	0.061	95%	0.037	0.107	192%
	% impr.	5%	2%		5%	2%	
10	50	0.035	0.062	79%	0.043	0.114	162%
	100	0.037	0.065	75%	0.047	0.118	149%
	% impr.	7%	5%		9%	3%	

Figure 3.5 visualizes the preceding results and helps make further comments. We observe that TCF increases almost linearly with the capacity levels of system components. Figure 3.6 shows the effect of the capacity levels of system components on ES and EP. We note from Figure 3.5 that similar TCF amounts can be obtained in different settings. For example, having 20 turbines together with $C_T = 10$ MWh and $C_C = C_D = 5$ MWh yields the TCF of 0.06 m\$. Having about 14 turbines with $C_T = 50$ MWh and $C_C = C_D = 5$ MWh also yields a similar TCF. This implies a trade-off between the number of turbines and the transmission line capacity. There exist similar trade-offs between all system components. The decision-maker has many system configuration options that lead to different operational decisions but similar TCF values. The decision-maker has this flexibility in the system design stage thanks to the substitution effect among different system components with respect to their capacity levels.

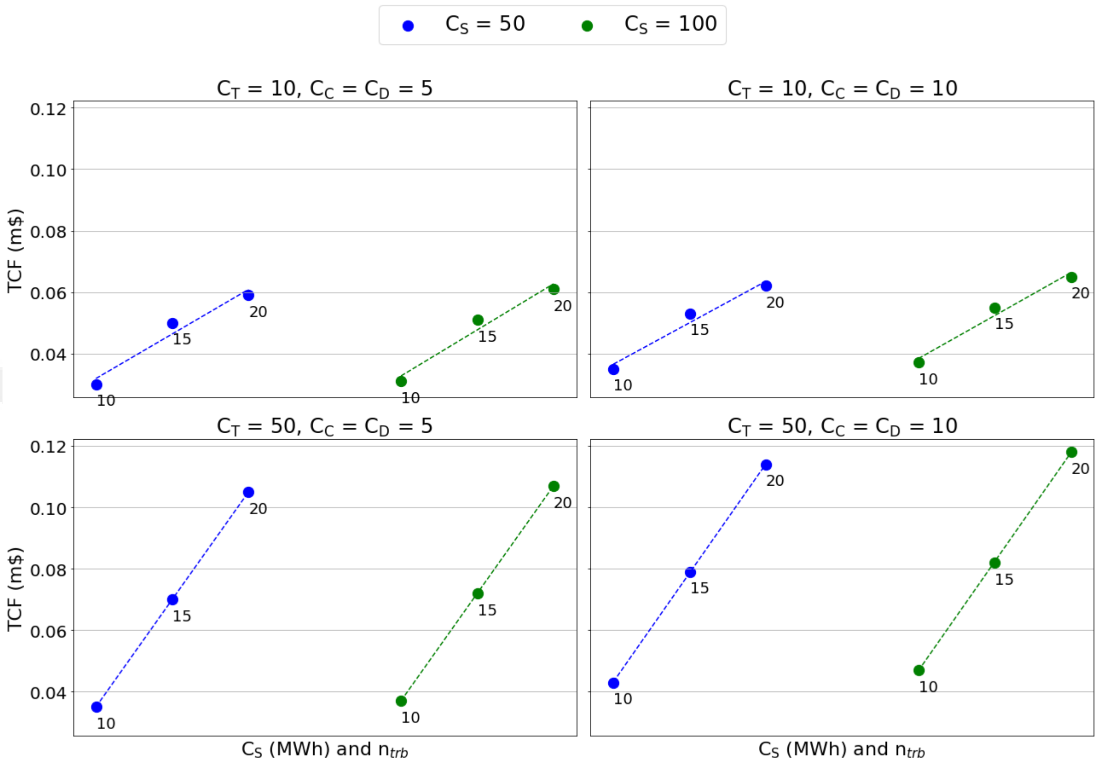

Figure 3.5: TCF values for different capacity levels of system components.

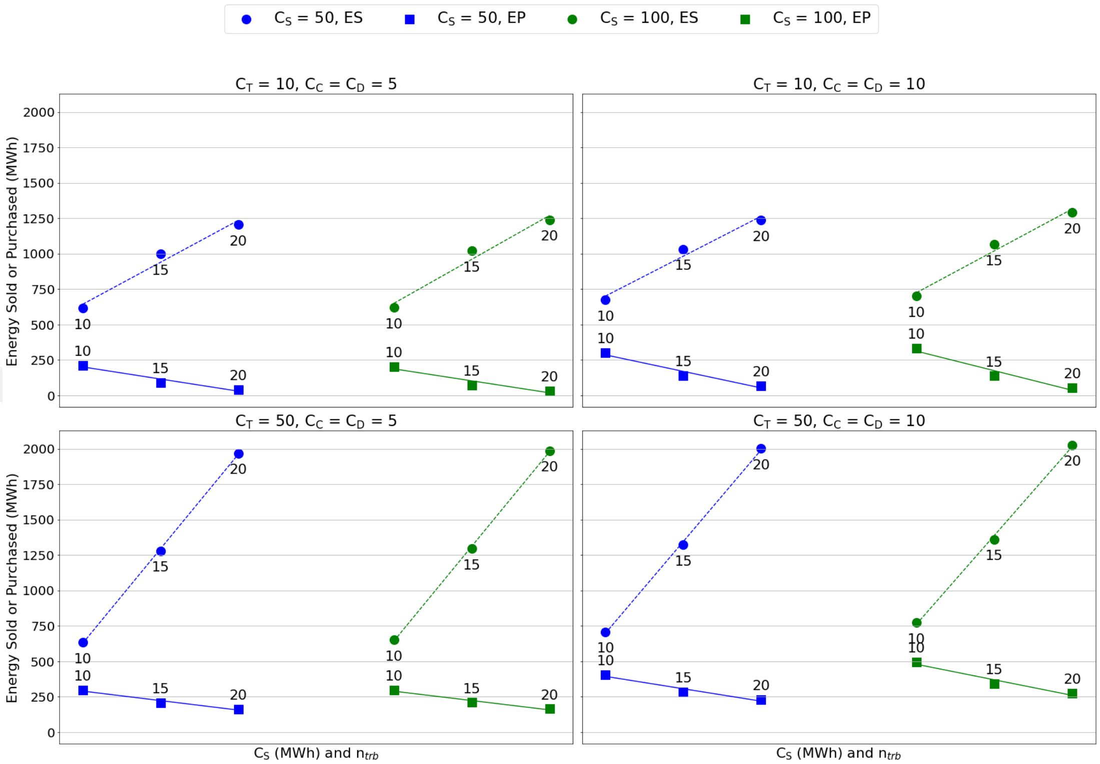

Figure 3.6: ES and EP values for different capacity levels of system components.

3.4 Further Numerical Analysis

In this section, we modify two key components of our energy system to quantify their effects on TCF. We first consider the case with no electricity demand and solve the energy generation and storage problem accordingly. See Subsection 3.4.1 for our results. In the absence of electricity demand, the system operator focuses more on selling electricity to the market and exploiting energy arbitrage opportunities. We then consider the case with no wind turbine and solve the energy generation and storage problem for the battery. See Subsection 3.4.2 for our results. In the absence of wind energy generation, the system operator relies only on market operations for demand fulfillment. More detailed results are given in Appendix B.

3.4.1 Case with No Electricity Demand

We analyze the effect of demand-fulfillment obligation on TCF by considering the setting in which the demand is zero throughout the planning horizon. We remove the demand component from the system, rerun all of our experiments, and compare our results with those of the original setting in Table 3.5. We observe that the demand component has a greater impact in smaller-sized systems. The TCF gain obtained by removing the demand component is 65% on average.

Table 3.5: Percentage TCF improvements when the demand component is removed from the system.

C_T	C_C=C_D	C_S	n_{trb}	w/ demand	no demand	**% impr.**
10	5	50	10	0.030	0.066	120%
			15	0.050	0.071	44%
			20	0.059	0.073	23%
		100	10	0.031	0.067	115%
			15	0.051	0.072	41%
			20	0.061	0.073	20%
	10	50	10	0.035	0.069	100%
			15	0.053	0.075	43%
			20	0.062	0.077	24%
		100	10	0.037	0.072	94%
			15	0.055	0.077	39%
			20	0.065	0.077	19%
50	5	50	10	0.035	0.082	136%
			15	0.070	0.118	68%
			20	0.105	0.153	45%
		100	10	0.037	0.084	130%
			15	0.072	0.119	66%
			20	0.107	0.130	21%
	10	50	10	0.043	0.091	110%
			15	0.079	0.126	60%
			20	0.114	0.161	42%
		100	10	0.047	0.095	101%
			15	0.082	0.130	58%
			20	0.118	0.165	40%

3.4.2 Case with No Wind Generation

We next examine the impact of wind farm on TCF by comparing the two settings in which the number of wind turbines is set to be ten and zero, respectively. See Table 3.6 for our results. Note that we have already shown the effect of doubling the number of turbines (from ten to twenty) in the previous section. The negative TCF values in the case with no wind generation implies that the energy arbitrage is not sufficient for system profitability since a large bulk of the energy capacity is spent to fulfill the demand.

Table 3.6: Percentage TCF losses when the wind farm is removed from the system.

C_T	C_C=C_D	C_S	$n_{trb}=10$	$n_{trb}=0$	**% loss**
10	5	50	0.030	-0.041	237%
		100	0.031	-0.039	226%
	10	50	0.035	-0.031	191%
		100	0.037	-0.028	176%
50	5	50	0.035	-0.037	206%
		100	0.037	-0.035	197%
	10	50	0.043	-0.028	165%
		100	0.047	-0.024	152%

3.5 Effect of Uncertainty

We will compare our solution approach with a deterministic one to measure the importance of including randomness in decision-making. We consider the setting in which the spike component of the price is ignored (but all the other random components are included) and compute the optimal cash flows via the recursion in Equation 3.7 for our instances in this setting. We then compute the value of stochastic solution (VSS): We consider the above setting by ignoring all uncertainties, replacing the random components for electricity demand, electricity price, and wind speed with their expected values, and solving the deterministic problem for our instances. The optimal policy for this deterministic problem is denoted by π^d. The TCF of policy π^d can be calculated from the recursion in Equation 3.7 constrained to take the actions of policy π^d in each state and each period. The TCF values of policy π^d are shown in column **D** of Tables 3.7 and 3.8. The optimal TCF values are shown in column **S** of Tables 3.7 and 3.8. From these TCF values, we compute the percentage VSS values using the formula %

VSS = $\frac{\textbf{S-D}}{\textbf{S}}$ x 100.

Table 3.7: VSS values when C_T = 10 MWh.

(a) $C_C = C_D = 5$

C_S	n_{trb}	**S**	**D**	% VSS
50	10	0.022	0.019	14%
	15	0.041	0.036	12%
	20	0.050	0.044	12%
100	10	0.023	0.020	15%
	15	0.042	0.036	14%
	20	0.052	0.044	14%

(b) $C_C = C_D = 10$

C_S	n_{trb}	**S**	**D**	% VSS
50	10	0.023	0.019	18%
	15	0.042	0.036	14%
	20	0.051	0.044	15%
100	10	0.025	0.020	20%
	15	0.044	0.036	18%
	20	0.054	0.044	19%

Table 3.8: VSS values when C_T = 50 MWh.

(a) $C_C = C_D = 5$

C_S	n_{trb}	**S**	**D**	% VSS
50	10	0.023	0.019	17%
	15	0.054	0.050	7%
	20	0.084	0.080	5%
100	10	0.025	0.020	18%
	15	0.055	0.051	8%
	20	0.086	0.081	5%

(b) $C_C = C_D = 10$

C_S	n_{trb}	**S**	**D**	% VSS
50	10	0.025	0.019	23%
	15	0.056	0.050	10%
	20	0.086	0.080	7%
100	10	0.028	0.020	27%
	15	0.059	0.051	13%
	20	0.089	0.082	9%

We note from Tables 3.7 and 3.8 that the percentage VSS values range between 5% and 27%. While no significant trend exists when the transmission line capacity is limited (C_T=10 MWh), increasing the number of wind turbines reduces the VSS value when transmission line capacity is high (C_T=50 MWh). The renewable energy scarcity makes the system more vulnerable to uncertainties and this impact is more evident in the presence of large transmission capacity. Also, increasing the storage capacity, the charge/discharge capacity, or the transmission line capacity raises the VSS value. Including randomness in decision-making is clearly more valuable in greater-sized systems.

3.6 Conclusion

In this study, we present an MDP formulation for the operational planning problem of a decentralized grid-connected system including a wind farm and a battery and having the primary objective of fulfilling the local electricity demand. We model the uncertainties in electricity demand, electricity price, and wind speed to implement them into our MDP formulation. We then solve the problem to optimality for realistic instances generated by varying the parameters of system components. We compute the optimal cash flows, amounts of energy sold/purchased, renewable energy generation, and average battery level in our instances.

Our results imply that the substitution effect among different system components provide flexibility in the system design choice: Different system configurations may lead to similar TCF values with different operational implications. For example, the decision-maker may consider increasing either the number of turbines or the transmission line capacity to improve TCF. However, the average battery storage level may increase with the number of turbines but may decrease with the transmission line capacity. We also observe that increasing the charge/discharge and storage capacities increases the amounts of energy sold and purchased. The impact of demand-fulfillment obligation on TCF is more significant when the system size is smaller. The absence of wind energy generation may render the energy arbitrage gains insufficient for positive TCF. Finally, we measure the value of including uncertainties in our problem setting, observing that the uncertainties gain more importance under renewable energy scarcity.

The insights provided in this chapter may inspire future work on sizing decisions for decentralized energy systems like ours. Future research may also consider wind power plants that are run with pumped-hydro energy storage facilities as an alternative storage unit to batteries. Since incorporating the streamflow rate and reservoir water levels increase the state space of the problem, heuristic solution methods such as deterministic re-optimization technique might be employed to deal with the additional computational burden of the MDP formulation. In addition, the design and operational planning problems might be jointly considered in a more complex optimization problem that will likely require more sophisticated solution methodologies.

Chapter 4

Conclusion

In this thesis, I have studied the design and operational planning problems of renewable energy systems with demand-fulfillment obligation. For the design problem, how the choice of PHES configuration affects the sizing and investment decisions of hybrid energy systems with solar/wind farms is investigated in Chapter 2. By generating scenarios for the streamflow rate from historical data and using the real data for the electricity demand, solar radiation, and wind speed, two-stage stochastic mixed-integer programming models that represent the system uncertainties are constructed. PHES systems are observed to help reduce the mismatched demand and thus the fossil-fuel usage. These systems are also more cost-effective than conventional hydropower systems. Open-loop PHES systems perform better than closed-loop and seawater PHES systems. Having natural inflow to the upper reservoir yields the lowest expected system cost for PHES and significantly reduces the fossil-fuel usage.

Chapter 3 considers a decentralized grid-connected wind farm-battery system with demand-fulfillment obligation. The energy generation and storage problem is formulated as an MDP that represents the electricity price, wind speed, and demand uncertainties via exogenous state variables. Solving the MDP with a backward recursion algorithm, the optimal energy generation and storage decisions are obtained. Trade-offs between system components are observed: differently sized system components may yield similar expected total revenues with different operational decisions. This substitution effect provides flexibility to the system operator in their system design choice. The demand-fulfillment obligation impacts the system profitability more when the system size is smaller. The absence of wind turbines would lead to negative cash flow values so that the energy arbitrage alone cannot profitably handle the demand-fulfillment obligation. The benefit of uncertainty modeling is greater when the renewable energy potential is limited.

This thesis suggests several potential directions for future research. Although the two-stage stochastic mixed-integer programming models in Chapter 2 enable us to offer insights into the PHES-design problem, stronger conclusions may be drawn by generating a higher number of scenarios to represent the electricity-demand, solar-radiation, and wind-speed uncertainties and including them in the models developed. The number of streamflow-rate scenarios may also be increased via scenario-generation algorithms. These extensions would increase the computational burden and may require decomposition algorithms to obtain the solutions. Another research direction is to approach the problem setting in Chapter 2 by leveraging the MDP methodology in Chapter 3. Since the stochastic programming model is a scenario-based approach, the available scenarios limit the uncertainty representation. The MDPs, on the other hand, are known to capture the real-life uncertainties better. Considering an MDP formulation for decentralized grid-connected PHES systems co-operated with solar/wind farms, one would come up with an augmented state space that may again induce high computational burden. Optimal policy structures may then be investigated to construct heuristic solution procedures to reduce the computational burden, as in [63] and [59].

Appendix A

Actual versus Predicted Demand Values

In this section, we compare the actual demand values with the predicted values. As the actual demand data is available only for the first size months of 2024, we use the months between January-June for our comparison. Predicted values are computed by deseasonalizing the demand values for the period 2021-2023 and adding back the previously computed seasonal components, for each period t. The values on the x-axes are the hours of the year, and in each Figure A.1-A.6, we use these hours to demonstrate periods in each month between January and June. The predicted values seem to be representing the actual values accurately.

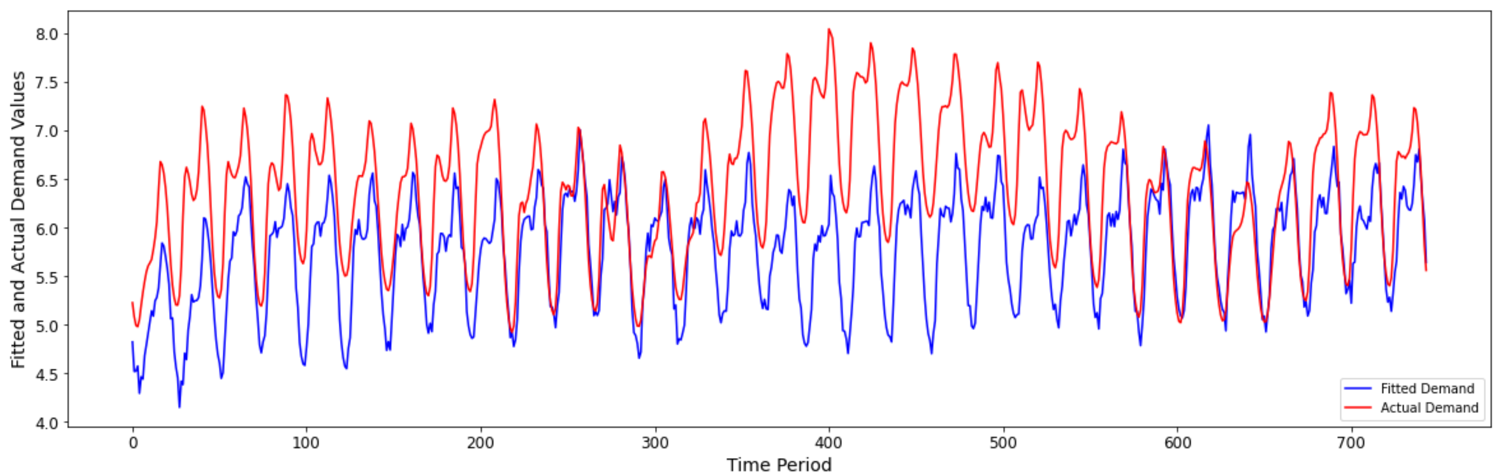

Figure A.1: Actual vs predicted demand values for January.

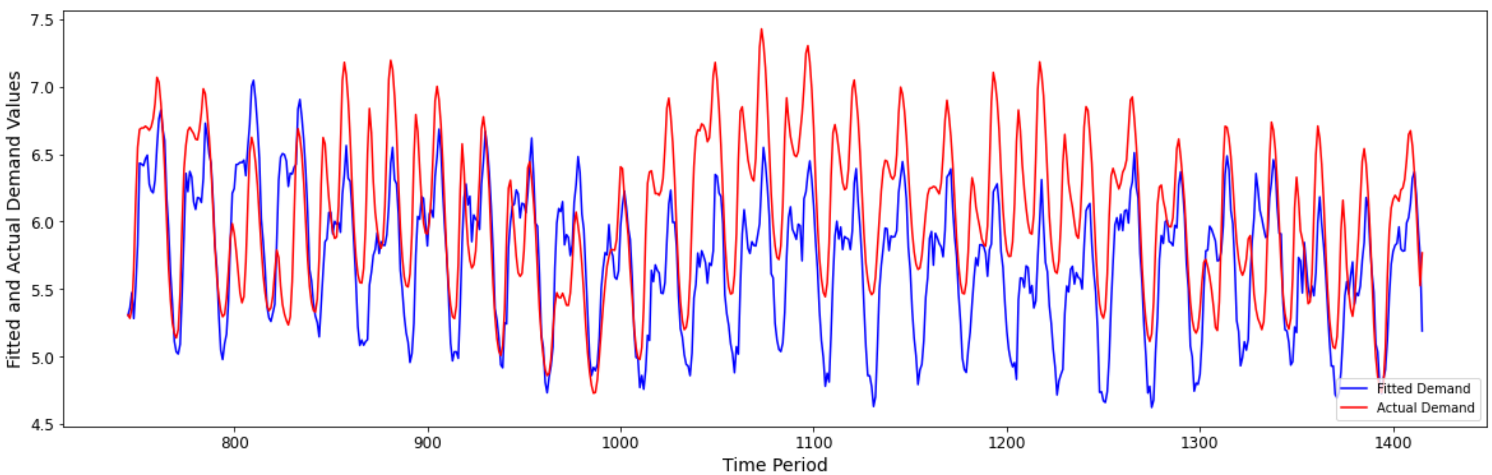

Figure A.2: Actual vs predicted demand values for February.

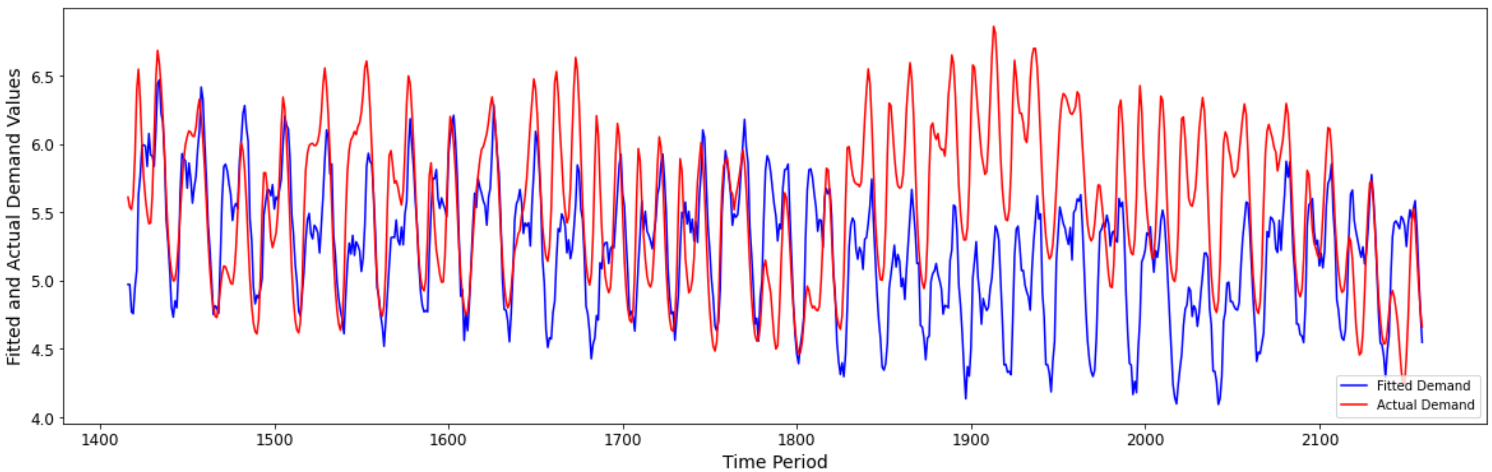

Figure A.3: Actual vs fitted demand values for March.

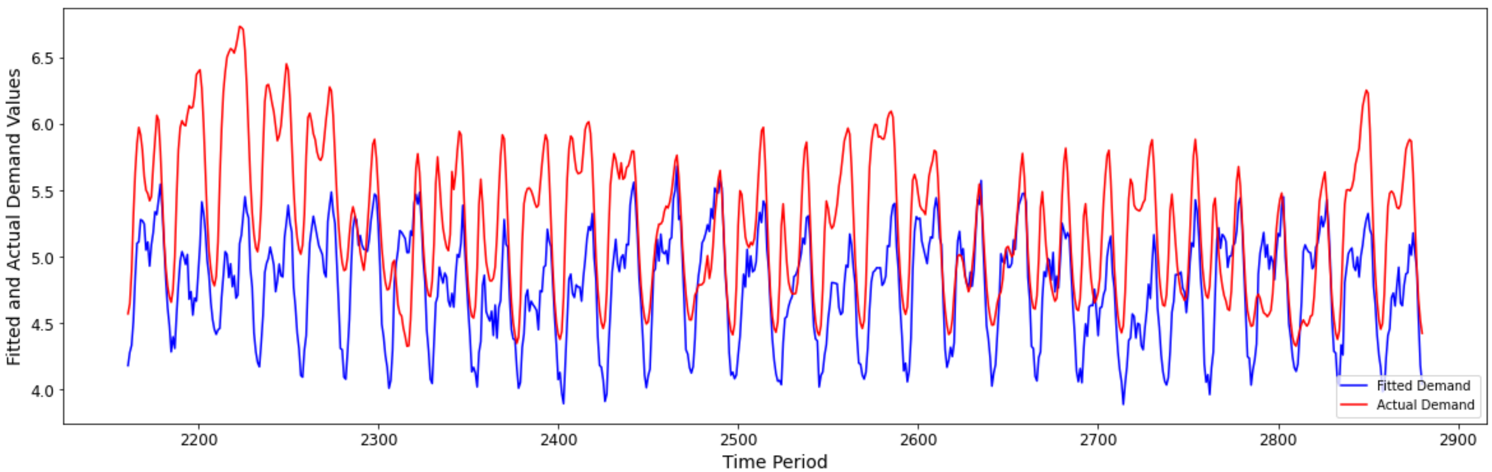

Figure A.4: Actual vs predicted demand values for April.

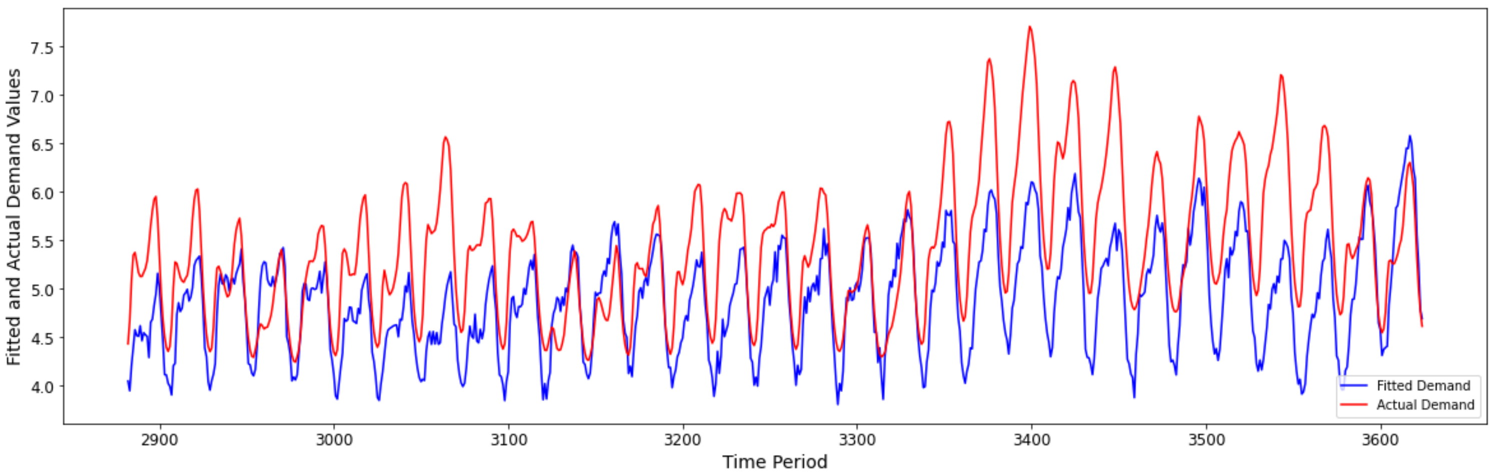

Figure A.5: Actual vs predicted demand values for May.

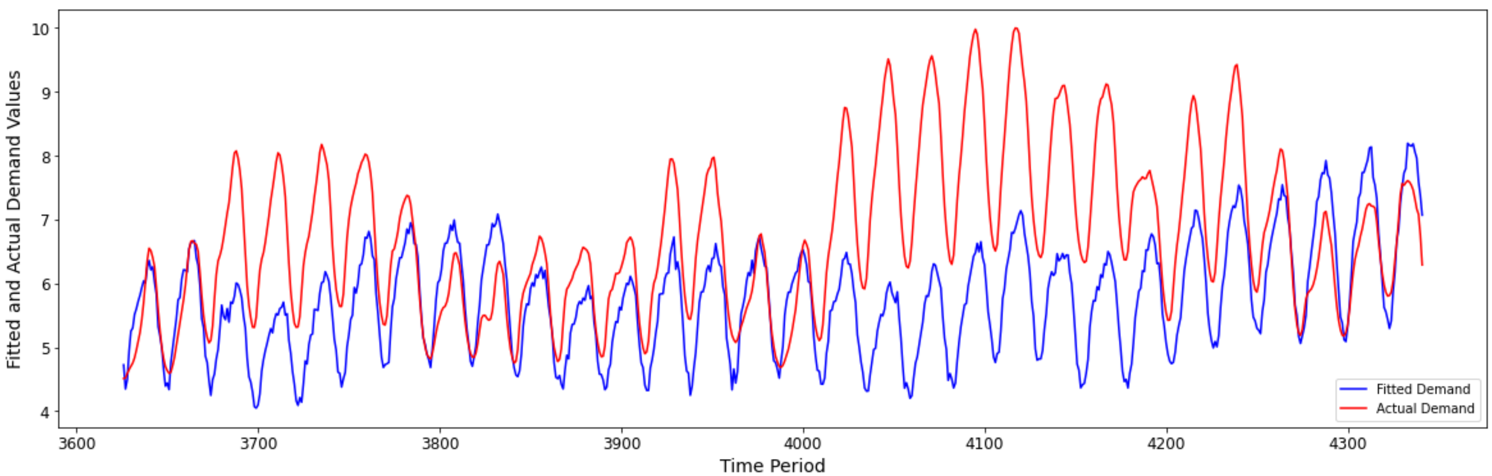

Figure A.6: Actual vs predicted demand values for June.

Appendix B

Tables for Further Numerical Analysis

We present in this section the TCF, ES, EP, RG, and BL metrics for the cases with no electricity demand and no wind generation. Table B.1 shows that EP values are low when there is the electricity demand is removed from the system, meaning that energy is purchased with very low or negative electricity prices only. Table B.2 shows the metrics for when there is no wind generation (i.e. the number of wind turbines is set to be zero). With extremely high EP and extremely low ES in the table, we comment that the cases with non-zero ES imply the arbitrage effect with adequate charging/discharging capacities, although that effect is not enough for the system to have non-negative cash flow values.

Table B.1: Metric results for the case in which the demand component is removed from the system.

C_T	C_C=C_D	C_S	n_{trb}	TCF	EP	ES	RG	BL
10	5	50	10	0.066	13	1344	1618	29
			15	0.071	2	1512	1913	35
			20	0.073	1	1560	1972	38
		100	10	0.067	10	1386	1699	53
			15	0.072	2	1531	1974	70
			20	0.073	1	1562	2001	77
	10	50	10	0.069	88	1344	1607	26
			15	0.075	65	1512	1918	29
			20	0.077	66	1555	2020	29
		100	10	0.072	93	1393	1703	51
			15	0.077	67	1553	2021	66
			20	0.077	68	1564	2078	65
50	5	50	10	0.082	60	1470	1701	25
			15	0.118	49	2191	2455	25
			20	0.153	45	2917	3208	25
		100	10	0.084	64	1491	1734	45
			15	0.119	52	2209	2487	45
			20	0.130	0	3035	3128	50
	10	50	10	0.091	134	1509	1785	26
			15	0.126	112	2219	2536	26
			20	0.161	100	2938	3286	26
		100	10	0.095	178	1537	1893	50
			15	0.130	140	2231	2648	50
			20	0.165	119	2941	3402	50

Table B.2: Metric results for the case in which the wind farm is removed from the system.

C_T	C_C=C_D	C_S	TCF	EP	ES	RG	BL
10	5	50	-0.041	1151	0	138	25
		100	-0.039	1131	0	164	43
	10	50	-0.031	1254	49	265	25
		100	-0.028	1272	67	338	48
50	5	50	-0.037	1176	0	197	25
		100	-0.035	1158	0	229	45
	10	50	-0.028	1263	54	270	25
		100	-0.024	1304	77	388	50

Bibliography

[1] Renewable Capacity Statistics 2022. Technical report, International Renewable Energy Agency, 2022.

[2] United Nations. Goal 7: Affordable and clean energy, 2015. URL `https://sdgs.un.org/goals/goal7`. Accessed: 2024-07-10.

[3] Sulman Shahzad and Elżbieta Jasińska. Renewable revolution: A review of strategic flexibility in future power systems. *Sustainability*, 16(13), 2024. ISSN 2071-1050.

[4] Gabrielle Coppez, Sunetra Chowdhury, and S.P. Chowdhury. The importance of energy storage in renewable power generation: A review. In *45th International Universities Power Engineering Conference UPEC2010*, pages 1–5, 2010.

[5] Xiaoshan Peng, Owen Q Wu, and Gilvan C Souza. Renewable, flexible, and storage capacities: Friends or foes? *Manufacturing & Service Operations Management*, 2024.

[6] Ekata Kaushik, Vivek Prakash, Om Prakash Mahela, Baseem Khan, Adel El-Shahat, and Almoataz Y. Abdelaziz. Comprehensive overview of power system flexibility during the scenario of high penetration of renewable energy in utility grid. *Energies*, 15(2), 2022. ISSN 1996-1073.

[7] Andrew Blakers, Matthew Stocks, Bin Lu, and Cheng Cheng. A review of pumped hydro energy storage. *Progress in Energy*, 3(2):022003, March 2021.

[8] Shafiqur Rehman, Luai M. Al-Hadhrami, and Md. Mahbub Alam. Pumped hydro energy storage system: A technological review. *Renewable and Sustainable Energy Reviews*, 44:586–598, 2015.

[9] A.G. Olabi, C. Onumaegbu, Tabbi Wilberforce, Mohamad Ramadan, Mohammad Ali Abdelkareem, and Abdul Hai Al–Alami. Critical review of energy storage systems. *Energy*, 214:118987, January 2021.

[10] 2022 Hydropower Status Report. Technical report, International Hydropower Association, 2022.

[11] 2021 Pumped Storage Report. Technical report, National Hydropower Association, 2021.

[12] Ayse Selin Kocaman and Vijay Modi. Value of pumped hydro storage in a hybrid energy generation and allocation system. *Applied Energy*, 205:1202–1215, November 2017.

[13] Julian David Hunt, Behnam Zakeri, Rafael Lopes, Paulo Sérgio Franco Barbosa, Andreas Nascimento, Nivalde José de Castro, Roberto Brandão, Paulo Smith Schneider, and Yoshihide Wada. Existing and new arrangements of pumped-hydro storage plants. *Renewable and Sustainable Energy Reviews*, 129:109914, September 2020.

[14] Rabea Jamil Mahfoud, Nizar Faisal Alkayem, Yuquan Zhang, Yuan Zheng, Yonghui Sun, and Hassan Haes Alhelou. Optimal operation of pumped hydro storage-based energy systems: A compendium of current challenges and future perspectives. *Renewable and Sustainable Energy Reviews*, 178:113267, 2023.

[15] Parinaz Toufani, Ece Cigdem Karakoyun, Emre Nadar, Olav B. Fosso, and Ayse Selin Kocaman. Optimization of pumped hydro energy storage systems under uncertainty: A review. *Journal of Energy Storage*, 73:109306, 2023.

[16] Parinaz Toufani, Emre Nadar, and Ayse Selin Kocaman. Short-term assessment of pumped hydro energy storage configurations: Up, down, or closed? *Renewable Energy*, 201:1086–1095, 2022.

[17] Parinaz Toufani, Emre Nadar, and Ayse Selin Kocaman. Operational benefit of transforming cascade hydropower stations into pumped hydro energy storage systems. *Journal of Energy Storage*, 51:104444, 2022.

[18] Menglian Zheng, Christoph J. Meinrenken, and Klaus S. Lackner. Smart households: Dispatch strategies and economic analysis of distributed energy storage for residential peak shaving. *Applied Energy*, 147:246–257, June 2015.

[19] Paul D. Brown, J. A. PeÇas Lopes, and Manuel A. Matos. Optimization of Pumped Storage Capacity in an Isolated Power System With Large Renewable Penetration. *IEEE Transactions on Power Systems*, 23(2):523–531, 2008.

[20] Wolf Heinrich Reuter, Sabine Fuss, Jana Szolgayová, and Michael Obersteiner. Investment in Wind Power & Pumped Storage in a Real Options Model– A Policy Analysis. *Renewable and Sustainable Energy Reviews*, 16 (4):2242–2248, 2012.

[21] Reza Hemmati. Stochastic energy investment in off-grid renewable energy hub for autonomous building. *IET Renewable Power Generation*, 13(12): 2232–2239, 2019.

[22] Jichun Liu, Jianhua Li, Yue Xiang, and Shuai Hu. Optimal Sizing of Hydro-PV-Pumped Storage Integrated Generation System Considering Uncertainty of PV, Load and Price. *Energies*, 12(15), July 2019.

[23] Ahmed Elnozahy, H.S. Ramadan, and Farag K. Abo-Elyousr. Efficient metaheuristic Utopia-based multi-objective solutions of optimal battery-mix storage for microgrids. *Journal of Cleaner Production*, 303:127038, 2021.

[24] Omar H. Abdalla, Life SMIEEE, Maged A. Abu Adma, and Abdelmonem S. Ahmed. Two-stage robust generation expansion planning considering long- and short-term uncertainties of high share wind energy. *Electric Power Systems Research*, 189:106618, 2020.

[25] Oluwamayowa O. Amusat, Paul R. Shearing, and Eric S. Fraga. Optimal design of hybrid energy systems incorporating stochastic renewable resources fluctuations. *Journal of Energy Storage*, 15:379–399, February 2018.

[26] Ayşe Selin Kocaman. Pompaj depolamalı hibrid enerji sistemi optimizasyonu-Türkiye için vaka analizi. *Gazi Üniversitesi Mühendislik Mimarlık Fakültesi Dergisi*, 34(1):53 – 68, 2019.

[27] Ayse Selin Kocaman, Carlos Abad, Tara J Troy, Woonghee Tim Huh, and Vijay Modi. A stochastic model for a macroscale hybrid renewable energy system. *Renewable and Sustainable Energy Reviews*, 54:688–703, 2016.

[28] Ayse Selin Kocaman, Emin Ozyoruk, Shantanu Taneja, and Vijay Modi. A stochastic framework to evaluate the impact of agricultural load flexibility on the sizing of renewable energy systems. *Renewable Energy*, 152:1067–1078, 2020.

[29] Özlem Çavuş, Ayşe Selin Kocaman, and Özlem Yılmaz. A risk-averse approach for the planning of a hybrid energy system with conventional hydropower. *Computers & Operations Research*, 126, February 2021.

[30] Homer Energy. URL `https://www.homerenergy.com/`.

[31] Onur Altıntaş, Büşra Ökten, Özlem Karsu, and Ayşe Selin Kocaman. Bi-objective optimization of a grid-connected decentralized energy system. *International Journal of Energy Research*, 42, September 2017.

[32] Enercon E-44. URL `https://en.wind-turbine-models.com/turbines/531-enercon-e-44`.

[33] John R. Birge and François Louveaux. *Introduction to Stochastic Programming*. Springer-Verlag, New York, NY, USA, 1997.

[34] Renewables 2023. Technical report, International Energy Agency (IEA), 2024.

[35] A.R. Dehghani-Sanij, E. Tharumalingam, M.B. Dusseault, and R. Fraser. Study of energy storage systems and environmental challenges of batteries. *Renewable and Sustainable Energy Reviews*, 104:192–208, 2019. ISSN 1364-0321.

[36] Anya Castillo and Dennice F. Gayme. Grid-scale energy storage applications in renewable energy integration: A survey. *Energy Conversion and Management*, 87:885–894, 2014. ISSN 0196-8904.

[37] Arne van Stiphout, Kristof De Vos, and Geert Deconinck. The impact of operating reserves on investment planning of renewable power systems. *IEEE Transactions on Power Systems*, 32(1):378–388, 2017.

[38] Aurobi Das and V. Balakrishnan. Grid-connectivity of remote isolated islands—A proposition in Indian context. *Journal of Renewable and Sustainable Energy*, 4(4):043119, 08 2012.

[39] Sonali Goel and Renu Sharma. Performance evaluation of stand alone, grid connected and hybrid renewable energy systems for rural application: A comparative review. *Renewable and Sustainable Energy Reviews*, 78:1378–1389, 2017. ISSN 1364-0321.

[40] Armin Razmjoo, Arezoo Ghazanfari, Poul Alberg Østergaard, and Sepideh Abedi. Design and analysis of grid-connected solar photovoltaic systems for sustainable development of remote areas. *Energies*, 16(7), 2023. ISSN 1996-1073.

[41] Muhammad Abdul Basit, Saad Dilshad, Rabiah Badar, and Syed Muhammad Sami ur Rehman. Limitations, challenges, and solution approaches in grid-connected renewable energy systems. *International Journal of Energy Research*, 44(6):4132–4162, 2020.

[42] Henok Ayele Behabtu, Maarten Messagie, Thierry Coosemans, Maitane Berecibar, Kinde Anlay Fante, Abraham Alem Kebede, and Joeri Van Mierlo. A review of energy storage technologies' application potentials in renewable energy sources grid integration. *Sustainability*, 12(24), 2020.

[43] Glen G. Farivar, William Manalastas, Hossein Dehghani Tafti, Salvador Ceballos, Alain Sanchez-Ruiz, Emma C. Lovell, Georgios Konstantinou, Christopher D. Townsend, Madhavi Srinivasan, and Josep Pou. Grid-connected energy storage systems: State-of-the-art and emerging technologies. *Proceedings of the IEEE*, 111(4):397–420, 2023.

[44] Md Masud Rana, Moslem Uddin, Md Rasel Sarkar, Sheikh Tanzim Meraj, G.M. Shafiullah, S.M. Muyeen, Md. Ariful Islam, and Taskin Jamal. Applications of energy storage systems in power grids with and without renewable energy integration — a comprehensive review. *Journal of Energy Storage*, 68:107811, 2023. ISSN 2352-152X.

[45] Mojgan Hojabri, Abu Zaharin Ahmad, Arash Toudeshki, and Mohammadsoroush Soheilirad. An overview on current control techniques for grid connected renewable energy systems. *International Proceedings of Computer Science and Information Technology*, 56:119, 2012.

[46] Dong Gu Choi, Daiki Min, and Jong-hyun Ryu. Economic value assessment and optimal sizing of an energy storage system in a grid-connected wind farm. *Energies*, 11(3), 2018.

[47] Mingzhen Song, Lingcheng Kong, and Jiaping Xie. Capacity investment decisions of energy storage power stations supporting wind power projects. *Industrial Management & Data Systems*, 123(11):2803–2835, 2023.

[48] Gulin Yurter, Emre Nadar, and Ayse Selin Kocaman. The impact of pumped hydro energy storage configurations on investment planning of hybrid systems with renewables. *Renewable Energy*, 222, 2024. ISSN 119906.

[49] Dibyendu Roy. Modelling an off-grid hybrid renewable energy system to deliver electricity to a remote indian island. *Energy Conversion and Management*, 281:116839, 2023. ISSN 0196-8904.

[50] Lorafe Lozano, Edward M. Querikiol, Michael Lochinvar S. Abundo, and Luzvisminda M. Bellotindos. Techno-economic analysis of a cost-effective power generation system for off-grid island communities: A case study of gilutongan island, cordova, cebu, philippines. *Renewable Energy*, 140:905–911, 2019. ISSN 0960-1481.

[51] Pikaso Pal and V. Mukherjee. Off-grid solar photovoltaic/hydrogen fuel cell system for renewable energy generation: An investigation based on techno-economic feasibility assessment for the application of end-user load demand

in north-east india. *Renewable and Sustainable Energy Reviews*, 149:111421, 2021. ISSN 1364-0321.

[52] Lilia Trisyathia Quentara and Erma Suryani. The development of photovoltaic power plant for electricity demand fulfillment in remote regional of madura island using system dynamics model. *Procedia Computer Science*, 124:232–238, 2017. ISSN 1877-0509. 4th Information Systems International Conference 2017, ISICO 2017, 6-8 November 2017, Bali, Indonesia.

[53] Binayak Bhandari, Sung-Hoon Ahn, and Tae-Bong Ahn. Optimization of hybrid renewable energy power system for remote installations: Case studies for mountain and island. *International Journal of Precision Engineering and Manufacturing*, 17(6):815–822, Jun 2016.

[54] Chouaib Ammari, Djamel Belatrache, Batoul Touhami, and Salim Makhloufi. Sizing, optimization, control and energy management of hybrid renewable energy system—a review. *Energy and Built Environment*, 3(4): 399–411, 2022.

[55] Raul Banos, Francisco Manzano-Agugliaro, FG Montoya, Consolacion Gil, Alfredo Alcayde, and Julio Gómez. Optimization methods applied to renewable and sustainable energy: A review. *Renewable and sustainable energy reviews*, 15(4):1753–1766, 2011.

[56] Saber Talari, Miadreza Shafie-khah, Gerardo J. Osório, Jamshid Aghaei, and João P.S. Catalão. Stochastic modelling of renewable energy sources from operators' point-of-view: A survey. *Renewable and Sustainable Energy Reviews*, 81:1953–1965, 2018. ISSN 1364-0321.

[57] Georgios N Psarros and Stavros A Papathanassiou. Generation scheduling in island systems with variable renewable energy sources: A literature review. *Renewable Energy*, 205:1105–1124, 2023.

[58] M Thirunavukkarasu, Yashwant Sawle, and Himadri Lala. A comprehensive review on optimization of hybrid renewable energy systems using various optimization techniques. *Renewable and Sustainable Energy Reviews*, 176: 113192, 2023.

[59] Ece Cigdem Karakoyun, Harun Avci, Ayse Selin Kocaman, and Emre Nadar. Deviations from commitments: Markov decision process formulations for the role of energy storage. *International Journal of Production Economics*, 255: 108711, 2023. ISSN 0925-5273.

[60] Yangfang Zhou, Alan Scheller-Wolf, Nicola Secomandi, and Stephen Smith. Electricity trading and negative prices: Storage vs. disposal. *Management Science*, 62(3):880–898, 2016.

[61] Michael Hassler. Heuristic decision rules for short-term trading of renewable energy with co-located energy storage. *Computers Operations Research*, 83: 199–213, 2017. ISSN 0305-0548.

[62] Daniel F Salas and Warren B Powell. Benchmarking a scalable approximate dynamic programming algorithm for stochastic control of grid-level energy storage. *INFORMS Journal on Computing*, 30(1):106–123, 2018.

[63] Yangfang (Helen) Zhou, Alan Scheller-Wolf, Nicola Secomandi, and Stephen Smith. Managing wind-based electricity generation in the presence of storage and transmission capacity. *Production and Operations Management*, 28(4): 970–989, 2019. doi: https://doi.org/10.1111/poms.12946.

[64] Harun Avci, E Cigdem Karakoyun, A Kocaman, Emre Nadar, and Parinaz Toufani. Integration of pumped hydro energy storage and wind energy generation: Structural analysis and algorithms. *Preprint http://dx. doi. org/10.13140/RG*, 2(17949.95200):1, 2021.

[65] Bo Yang, Selvaprabu Nadarajah, and Nicola Secomandi. Least squares monte carlo and pathwise optimization for merchant energy production. *Operations Research*, 2023.

[66] U.S. Energy Information Administration. Hourly electric grid monitor - new york region, 2024. URL `https://www.eia.gov/electricity/gridmonitor/dashboard/electric_overview/regional/REG-NY`. Accessed: 2024-06-17.

[67] Robert B Cleveland, William S Cleveland, Jean E McRae, Irma Terpenning, et al. Stl: A seasonal-trend decomposition. *Journal of Official Statistics*, 6 (1):3–73, 1990.